Targeted Dab2 Restoration: A Novel Approach for Enhanced Wound Healing in Diabetic Conditions

Sudarshan Bhattacharjee [1, 2], Hao Wu [1, 2], Beibei Wang [1, 2], Kui Cui [1, 2], Shahram Eisa-Beygi [1], Donghai Wang [1], Douglas B Cowan [1, 2], Scott Wong [1], Jinjun Shi [3, 4], Hong Chen [1, 2],

Affiliations

- [1] Vascular Biology Program (S.B., Y.D., B.W., K. Cui, H.W., D.W., S.W., H.C.), Boston Children's Hospital, MA.
- [2] Departments of Surgery (Y.D., B.W., K. Cui, S.B., H.C.), Harvard Medical School, Boston, MA.
- [3] Department of Anesthesia (J.S.), Harvard Medical School, Boston, MA.
- [4] Department of Anesthesiology, Perioperative and Pain Medicine, Brigham and Women's Hospital, Boston, MA (J.S.).

Abstract

This study investigates the molecular underpinnings of endothelial dysfunction in diabetes, focusing on the roles of Disabled-2 (Dab2) and Forkhead Box M1 (FoxM1) in VEGFR2 signaling and endothelial cell function. Our research reveals critical insights into the downregulation of Dab2 and FoxM1 in endothelial cells (ECs) under hyperglycemic conditions that leads to impaired angiogenesis and delayed wound healing. These findings Substantiate our hypothesis that restoring Dab2 expression through targeted therapies could enhance angiogenesis and wound repair in diabetic environments.

In vitro experiments involved treating primary murine brain ECs with high glucose concentrations, simulating hyperglycemic conditions in diabetes mellitus. Bulk RNA-sequencing analysis identified significant downregulation of Dab2, FoxM1, and genes involved in cell cycle progression, cell growth, survival, glycolysis, and oxidative phosphorylation. In vivo, ECs isolated from diabetic mice showed a marked decrease in Dab2 and FoxM1 compared to controls, validated by immunostaining and western blot analysis. Notably, FoxM1 was found to directly bind to the Dab2 promoter, regulating its expression and influencing VEGFR2 signaling.

Dab2 deficiency led to enhanced lysosomal degradation of VEGFR2 in high-glucose-treated ECs, reducing VEGFR2 signaling. This was further supported by in vitro experiments showing decreased proliferation and angiogenic capability in Dab2-deficient brain ECs. Correspondingly, diabetic mice lacking Dab2 exhibited slower wound healing and reduced neovascularization.

To explore therapeutic potential, we employed Dab2-mRNA encapsulated in lipid nanoparticles, significantly improving wound healing and angiogenesis in diabetic mice. This study provides substantial evidence of the crucial roles of Dab2 and FoxM1 in diabetic endothelial dysfunction and proposes targeted gene delivery systems as a promising treatment for diabetic vascular complications.

Introduction

Diabetes mellitus, a multifaceted metabolic disorder characterized by chronic hyperglycemia, is a predominant global health concern due to its increasing prevalence and association with a spectrum of complications, particularly in vascular health (1,2,3). One of the critical yet understudied aspects of diabetic complications is the impairment of wound healing, a process inherently reliant on efficient vascular responses, including angiogenesis and endothelial cell function (4,5,6). At the heart of vascular homeostasis and repair are endothelial cells (ECs), which form the inner lining of blood vessels and are central to angiogenesis, the formation of new blood vessels from pre-existing ones. Understanding the molecular mechanisms that underpin endothelial dysfunction in diabetes is crucial for developing targeted therapeutic strategies.

A pivotal player in the regulation of endothelial function and angiogenesis is the Vascular Endothelial Growth Factor (VEGF) and its receptors, particularly VEGFR2. The VEGF-VEGFR2 signaling pathway is instrumental in mediating endothelial cell proliferation, migration, and new vessel formation, processes vital for wound healing and tissue regeneration (7,8,9). In the context of diabetes, the functionality of this pathway is severely compromised, leading to diminished angiogenesis and delayed wound healing (10,11,12). However, the intricate molecular mechanisms that lead to these dysfunctions in diabetic conditions are not entirely understood.

Recent research has highlighted the potential role of Dab2, a key adaptor protein involved in endocytic and signaling pathways, in modulating VEGFR2 signaling and, by extension, angiogenesis. Dab2 interacts with several intracellular proteins to regulate processes such as cell migration, adhesion, and proliferation — all of which are crucial for effective angiogenesis and wound healing (13,14,15). Notably, alterations in Dab2 expression and function have been associated with various pathological conditions, including cancer and cardiovascular diseases (16,17). However, its role in diabetes-induced vascular complications, particularly impaired wound healing, has not been extensively explored.

Concomitantly, FoxM1, a transcription factor known to promote cell cycle progression, cell proliferation, and metabolism, has been implicated in vascular development and pathology (18,19,20,21). Its regulatory relationship with Dab2 and subsequent effects on VEGFR2 signaling in diabetic conditions is an area ripe for investigation. The possibility that FoxM1 directly influences Dab2 expression and thereby modulates VEGFR2-mediated endothelial function presents a novel avenue for understanding and potentially mitigating the vascular complications of diabetes.

This study posits that in diabetic conditions, characterized by high glucose environments, the expression of Dab2, and consequently the VEGFR2 signaling, is significantly downregulated, leading to impaired angiogenesis and delayed wound healing. We hypothesize that restoring Dab2 expression through targeted therapies could rescue the impaired angiogenesis and enhance wound healing in diabetic conditions. To this end, we investigated the expression levels of Dab2 and FoxM1 in high glucose-treated ECs and in ECs isolated from diabetic mice. Furthermore, we explored the regulatory relationship between FoxM1 and Dab2 and the subsequent impact on VEGFR2 signaling and endothelial function.

In pursuit of a therapeutic strategy, we designed a novel rescue experiment employing Dab2-mRNA encapsulated in lipid nanoparticles conjugated with Lrp1 peptide. This treatment aimed

to restore Dab2 expression in diabetic mice and, in turn, rescue the impaired angiogenic response and wound healing. The potential of this approach was assessed in streptozotocin (STZ)-induced diabetic mice, a well-established model for studying diabetes and its complications (22,23,24). The efficacy of Dab2-mRNA treatment was evaluated based on the rate of wound closure and the extent of angiogenesis in treated versus untreated diabetic mice.

Furthermore, to provide a robust foundation for our in vivo findings and to understand the underlying cellular mechanisms, we conducted in vitro experiments using a Dab2-Lenti system in Dab2 knockout and high glucose-treated primary brain endothelial cells from mice. These studies aimed to dissect the role of Dab2 in endothelial cell migration, proliferation, and tube formation — key processes in angiogenesis and wound healing.

The overarching goal of this research is to elucidate the molecular mechanisms by which Dab2 and FoxM1 modulate VEGFR2 signaling and endothelial function in diabetic conditions and to explore the therapeutic potential of restoring Dab2 expression for enhancing angiogenesis and wound healing in diabetes. By addressing these objectives, this study aims to contribute significantly to our understanding of diabetic vascular complications and to pave the way for novel therapeutic approaches to mitigate these severe outcomes.

Methods:

Cell culture:

Primary mouse endothelial cells were obtained from either mouse skin or brains and cultured according to previously established protocols. Briefly, to isolate MECs from the skin, 4-6 mice aged 2-3 months were used. The mice were anesthetized with isoflurane and humanely euthanized by cervical dislocation. The skin was excised from the mice using surgical scissors or a scalpel, then diced into small fragments and subjected to enzymatic digestion with collagenase Type IV (2 mg/ml; Gibco Laboratories) in a 37°C water bath with agitation for a duration of 60-90 minutes. The digestion process was stopped by adding an equal volume of fetal bovine serum (FBS). The resulting digested tissue was filtered through a 40 µm cell strainer to separate the cells from debris. The resulting cell suspension was then centrifuged at x g for x minutes at 4°C. The isolated pellet was re-suspended in a buffer (x) and subjected to labeling with anti-mouse CD31. Magnetic-activated cell sorting (MACS) was employed to isolate endothelial cells from the cell suspension. The isolated cells were then utilized for downstream experiments. To isolate MECs from the brain, meninges were carefully removed from 2-3 month-old mice's forebrain and gray matter was minced. The minced tissue was then digested with 2 mg/ml collagenase Type IV (2 mg/ml; Gibco Laboratories) in DMEM (Sigma-Aldrich) containing 50 mg/ml gentamicin and 2 mM glutamine in a 37°C water bath for 1 hour. After digestion, the tissue was stopped by adding an equal volume of fetal bovine serum (FBS) and

then filtered through a cell strainer (pore size: x µm) to remove debris. The resulting cell suspension was centrifuged at x g for x minutes at 4°C to pellet the cells. Endothelial cells derived from wild-type mice or mice carrying Dab2 fl/fl; iCDH5-ER T2 Cre (Dab2 fl/fl/iCDH5-ER T2 Cre) alleles were exposed to 5 µM of 4-hydroxytamoxifen (dissolved in ethanol) for a duration of two days at 37°C. Following this treatment, the cells were incubated for another two days without 4-hydroxytamoxifen. Confirmation of Dab2 deletion was carried out by Western blot using VEGFR2 antibody. The primary MECs used in all experiments were isolated and maintained between 1-5 passages. Cells were treated with normal glucose (5 mM) or high glucose (25 mM) medium for 24 hours. There were no significant differences observed between MECs isolated from the skin and brain.

Dab2 KO mice:

To produce EC-specific Dab2KO mice, a breeding strategy was employed using Dab2fl/fl mice and EC-specific Cre transgenic CDH5-Cre mice. The Dab2fl/fl mice were homozygous for a floxed Dab2 gene, while the EC-specific CDH5-Cre mice expressed the Cre recombinase enzyme. The breeding resulted in offspring with the Dab2 gene specifically deleted in the endothelial cells through the action of the Cre recombinase. The final mice population, EC-specific Dab2KO mice, was characterized by a specific knockout of the Dab2 gene in the endothelial cells.

RNA isolation and quality control:

Total RNA was isolated from the cells using a commercially available kit (Qiagen, Valencia, CA, USA) according to the manufacturer's instructions. RNA quantity and quality were determined using a NanoDrop 2000 spectrophotometer (Thermo Fisher Scientific, Waltham, MA, USA) and an Agilent 2100 Bioanalyzer (Agilent Technologies, Santa Clara, CA, USA).

Library preparation and sequencing:

RNA sequencing libraries were prepared using the Illumina TruSeq Stranded mRNA Library Prep Kit (Illumina, San Diego, CA, USA) according to the manufacturer's instructions. Briefly, poly(A)+ RNA was purified using oligo(dT) magnetic beads and fragmented. cDNA was synthesized using reverse transcriptase and random primers, followed by second-strand synthesis. The double-stranded cDNA was then subjected to end-repair, A-tailing, and ligation of Illumina sequencing adapters. The libraries were amplified by PCR and purified using Agencourt AMPure XP beads (Beckman Coulter, Brea, CA, USA). The quality and quantity of the libraries were assessed using an Agilent 2100 Bioanalyzer and qPCR. The libraries were then sequenced on an Illumina HiSeq 2500 sequencing platform (Illumina, San Diego, CA, USA) to generate paired-end reads of 100 bp length.

Data analysis:

The raw sequencing data were preprocessed to remove low-quality reads and adapter sequences using FastQC and Trimmomatic software. The high-quality reads were aligned to the human reference genome (GRCh38) using the HISAT2 aligner. Gene expression levels were quantified using the featureCounts software. Differential gene expression analysis was performed using the edgeR package. The differentially expressed genes were identified based on the fold change (FC) and false discovery rate (FDR) cutoffs of 2 and 0.05, respectively. The gene ontology (GO) and pathway enrichment analysis were performed using the DAVID and KEGG databases.

qRT-PCR:

Total RNA was isolated from primary mouse endothelial cells using a commercially available kit (Qiagen, Valencia, CA, USA) followed by DNase I treatment. The RNA was then reverse transcribed into cDNA using Oligo (dT) 20 Primers (Invitrogen-18418-020) as per the manufacturer's protocol. Quantitative real-time PCR was performed using the StepOnePlus Real-Time PCR detection system (Applied Biosystems, Foster City, CA, USA) and Platinum SYBR Green qPCR super Mix (Invitrogen). The PCR amplification cycles consisted of an initial heating step at 95°C for 10 min, followed by 40 cycles of 15 s at 95°C, 1 minute at 60°C, and 45 s at 72°C. The relative abundance of mRNA was determined using the average threshold cycles (Ct) of samples normalized to β-actin mRNA. Each sample was analyzed in triplicate. The following primer sequences were used for PCR: Dab2 (antisense primer, 5'-GTGAGGTCGGCAATCTCTGA-3', and the sense primer, 5'-AGATCAAGGTTCGAGAGGCCA-3'), FoxM1 (antisense primer, 5'-GGGACAGATTGTACGGTGGC-3', and the sense primer, 5'TCTCTCCCACAGCAGACTACG-3'), GATA1 (antisense primer, 5'-GGAGTTTGTGGTGGGGAGAG', and the sense primer, 5'-ACATCCCAGGTTTTAGGCCG-3'), and β-actin (antisense primer, 5'-AGCACTGTGTTGGCGTACAG-3', and the sense primer, 5'-AGAGCTACGAGCTGCCTGAC-3').

RNA Interference:

The study used RNA interference (RNAi) to knockdown the expression of specific genes in primary brain ECs. The cells were transfected with siRNA duplexes using either Oligofectamine or RNAiMAX, according to the manufacturer's instructions (Invitrogen; 12252-011, 13778-150). The study used a mouse Dab2 (Sense: GGGAAUACCCUUCUUCGAATT; Anti-Sense: UUCGAAGAAGGGUAUUCCCTT), and its respective scrambled control siRNA, which were purchased from Invitrogen. The cells were processed for biochemical immunoprecipitation or immunofluorescence assays 48-72 hrs after transfection, as previously described.

Dab2-mRNA-LNPs injection to mice

We encapsulated Dab2 mRNA within lipid nanoparticles to form a targeted gene therapy tool. These LNPs were additionally attached to Lrp1 peptide to improve the precision of their

delivery specifically to the glomerular endothelial cells in the kidneys. This encapsulation process was crucial to maintain the stability and effectiveness of the Dab2 mRNA for its use in living organisms (in vivo). The prepared Dab2-mRNA-LNPs were administered to mice through an intravenous (i.v.) injection, with a dosage of 15 µg per mouse. This treatment was given twice a week for a total of four weeks. To confirm the accuracy of our LNP delivery system, we conducted a parallel experiment. In this experiment, we used Cyanine-5 (Cy5), a fluorescent dye, encapsulated in similar Lrp-1-conjugated LNPs. We observed the distribution of Cy5 in the kidney glomeruli of healthy mice, which indicated the successful targeting of the LNPs.

Western Blot:

To extract total proteins, cells were lysed using RIPA buffer. Equal amounts of denatured protein were loaded onto a 10% SDS-PAGE gel for electrophoresis. The separated proteins were then transferred to a PVDF membrane and blocked with 5% skimmed milk for 30 minutes at room temperature. Primary antibodies were added to the membrane and incubated overnight at 4°C. The membrane was then incubated with a secondary antibody for 2 hours at room temperature. Bands were detected using the classical X-ray film method. The experiment was repeated three times. The primary antibody was diluted at 1:1,000, and the secondary antibody was diluted at 1:2,000.

Immunofluorescence:

For immunofluorescence staining, primary mouse endothelial cells were cultured on glass coverslips and fixed in 4% paraformaldehyde (PFA) for 10 minutes. The cells were then permeabilized with 0.3% Triton X-100 in phosphate-buffered saline (PBS) for 10 minutes and blocked in a blocking solution containing 5% donkey serum in PBS for 1 hour at room temperature. The primary antibodies were diluted in blocking solution and incubated with the cells overnight at 4°C. The next day, the coverslips were washed with PBS and incubated with the respective secondary antibodies conjugated to fluorescent labels (Alexa Fluor) for 2 hours at room temperature. After washing with PBS, the coverslips were mounted on glass slides using Vectashield mounting medium with DAPI and visualized using a fluorescence microscope (Zeiss LSM 880) with appropriate filters. Images were acquired using a digital camera (Zeiss AxioCam).

Scratch assay:

An in vitro scratch wound healing assay was performed to evaluate the migration of wild type and EC-specific Dab2KO cells under normoglycemic and hyperglycemic conditions. Cells were seeded in a 24-well plate and grown to confluence. A scratch wound was made in the cell monolayer using a sterile pipette tip, and the cells were washed to remove any detached cells. The cells were then cultured in either a normoglycemic media (5 mM glucose) or a

hyperglycemic media (20 mM glucose) in presence or absence of VEGF-A (100ng/ml) and images were taken at specified time points to monitor cell migration into the wound area. The rate of cell migration was calculated by measuring the width of the wound at different time points. The differences in wound closure between wild type and EC-specific Dab2KO cells under both normoglycemic and hyperglycemic conditions were analyzed.

Network formation assay:
An in vitro matrigel assay was performed to compare the behavior of wild type and EC-specific Dab2KO cells in normoglycemic and hyperglycemic conditions. The cells were seeded on top of a matrigel matrix in a 24-well plate, and cultured in a normoglycemic media (5 mM glucose) or a hyperglycemic media (20 mM glucose) for a specified period of time. The cells were fixed and analyzed to determine morphological changes and quantify cell migration and proliferation. The differences in behavior between the wild type and EC-specific Dab2KO cells were analyzed under both normoglycemic and hyperglycemic conditions.

EdU staining:
An EdU staining assay was performed to determine the cell proliferation of wild type and EC-specific Dab2KO cells under normoglycemic and hyperglycemic conditions. The cells were cultured in either a normoglycemic media (5 mM glucose) or a hyperglycemic media (20 mM glucose) and then incubated with EdU, a thymidine analog, for 4 hours in presence or absence of VEGF-A (100ng/ml). The cells were then fixed and processed for staining, including the addition of a DAPI stain to visualize the nuclei. The EdU-incorporated cells were identified by fluorescence using a specific antibody. The number of EdU positive cells was counted and compared between the wild type and EC-specific Dab2KO cells under both normoglycemic and hyperglycemic conditions. The differences in cell proliferation were analyzed and quantified.

Wound healing in mice:
A dermal wound healing assay was performed to evaluate the role of the Dab2 gene in the wound healing process. Two groups of mice, wild type and EC-specific Dab2KO, were used in this study. A standardized wound was created on the dorsal surface of each mouse using a surgical blade. The mice were then monitored for a specified period of time to evaluate wound healing, including changes in wound size and tissue regeneration. At the end of the study, the mice were sacrificed and the wound sites were collected for further analysis. The collected tissue was processed for histological analysis, including the use of specific stains to evaluate tissue regeneration and wound healing progression. The differences in wound healing response between the wild type and EC-specific Dab2KO mice were analyzed and quantified. This assay provided valuable information on the role of the Dab2 gene in regulating wound healing in vivo.

Matrigel plug assay:

An in vivo matrigel assay was performed to study the angiogenic response of wild type and EC-specific Dab2KO mice. Matrigel mixed with 100 ng/ml VEGF-A was prepared and a specified volume was implanted subcutaneously into the back of both wild type and EC-specific Dab2KO mice. The mice were then monitored for a specified period of time to evaluate angiogenic response, including the formation of blood vessels in the implantation site. At the end of the study, the mice were sacrificed and the implantation sites were collected for further analysis. The collected tissue was processed for histological analysis, including the use of specific stains to visualize blood vessels and quantify angiogenic response. The differences in angiogenic response between the wild type and EC-specific Dab2KO mice were analyzed and quantified. This assay provided valuable information on the role of the Dab2 gene in modulating angiogenic response in vivo.

Statistics:

The statistical analysis was conducted using GraphPad Prism 9 or SPSS (IBM) software and the data is presented as mean ± SEM. Multiple comparisons were performed using one-way ANOVA and two-way ANOVA followed by Tukey's post hoc analysis when appropriate. A P-value of less than 0.05 was considered statistically significant. Additionally, the two-tailed student's t-test was used for individual comparisons.

Results

High concentration of glucose treatment of ECs down-regulates the expression of Dab2, FoxM1, as well as genes involved in cell cycle progression, cell growth and survival, glycolysis and oxidative phosphorylation

To elucidate the gene regulatory network in ECs during vascular development in diabetes, we treated primary murine brain endothelial cells with normal or high glucose concentrations (20 mM, a condition mimicking hyperglycemia in diabetes mellitus) for a period of 48 hours, followed by bulk RNA-sequencing analysis. Differential gene expression revealed 168 significantly downregulated and 386 significantly up-regulated genes in the high-concentration glucose treated ECs compared to ECs cultured in normal glucose media (Fig 1a). The volcano plot analysis identified the downregulation of the Dab2 gene in high glucose-treated ECs compared to the control group (Fig1a). Volcano plot of transcription factors revealed that transcription factors that regulates cell proliferation and growth, including FoxM1, Egr2 (Early growth response protein 2), Hes1 (Hairy and enhancer of split 1), Etv4 (ETS variant 4), were downregulated in high glucose-treated samples compared to control (Fig 1b). The

downregulation of genes in high-concentration glucose treated ECs compared to controls was further confirmed by quantitative PCR (qPCR)(Fig 2a-d*).*
Geneset enrichement identified multiple down-regulated genesets by high-concentration glucose treatment that are involved in the regulation of cell cycle proression such as E2F target genes, G2-M checkpoint, and mitotic spindle formation; or cell growth such as mTORC1 signaling and Myc target genes (Fig.1c). Consistent with the down regulation of Myc target genes that include a vast majority of metabolic genes, metabolic process including glycolysis and oxidative phosphorylation are also downregulated in ECs treated with high concentration of glucose (Fig.1c). This suggests that the aerobic glycolysis, a process usually coupled with cell proliferation and growth is impaired in the presence of high concentration of glucose. *(Please replace the angiogenic Enrichment plot in Fig.1d with that of E2F targets or G2M, or Myc).*
Taken together, those *in vitro* observations suggest that ECs exposed to hyperglycemia downregulated the expression of Dab2 and FoxM1 as well as genes involved in cellular metabolism, growth, and proliferation.

Decreased expression of FoxM1 and Dab2 in ECs isolated from diabetic mice
FoxM1 has been shown to promote cell cycle progression, cell proliferation and cellular metabolism whilst Dab2 is a critical regulator of VEGFR2 signaling. Downregulation of both FoxM1 and Dab2 in ECs exposed to high glucose conditions *in vitro* (Fig. 1a &1b) prompted us to look at the expression level of those two genes in ECs from diabetic mice which are constantly exposed to hyperglycemia. Indeed, in skin and brain ECs isolated from mice with STZ-induced diabetes mellitus, the abundance of both *Dab2* and *Foxm1* were lower compared to healthy controls (Fig. 2a-c). Consistently, western blot analysis revealed significantly low levels of Dab2 and FoxM1 in diabetic groups compared to non-diabetic controls (Fig.2e). Down regulation of Dab2 expression in diabetic conditions was confirmed by immunostaining of brain ECs cultured in normal or high glucose concentrations (Fig.2g). To further validated those findings, we examined the growing blood vessels from VEGFA-infused matrigels from WT and diabetic mice and found a significant reduction in Dab2 levels in the diabetic group compared to the WT group (Fig. 2h). Together, those data demonstrated that Dab2 as well as FoxM1 are down regulated in ECs exposed to high concentrations of glucose both *in vivo* and *in vitro*.

FoxM1 directly binds to *Dab2* promoter region and regulates its expression
FDI-6 is a FoxM1 transactivational inhibitor that blocks its DNA binding capacity (PMID: 34206484, PMID: 34880209). Immunostaining revealed a significant decrease in the expression of pVEGFR2 and Dab2 in FDI-6-treated ECs compared to control, while the expression of FoxM1 remained unchanged (Fig 3a). This observation was confirmed by western blot analysis of brain ECs stimulated with VEGFA, which showed that FDI-6 treatment reduced the protein levels of both phosphorylated form of VEGFR2 (pVEGFR2) and Dab2, as well as compromised activation

of both ERK and AKT (Fig 3b). In contrast, the protein level of FoxM1 was not affected by FDI-6 treatment. Those observations suggest that FoxM1 regulates the expression of Dab2 which in turn controls VEGFR2 signaling.

To investigate how FoxM1 regulates Dab2 expression and VEGFR2 signaling, we determined whether FoxM1 can bind to Dab2-promoter and other regulatory regions by ChIP-qPCR analysis in brain ECs. JASPAR (a reference is required for this) was used to predict potential FoxM1 transcription factor binding sites, and two potential binding sites within the promoter region of *Dab2* locus with the highest score were selected for further study (Fig 3c, e). Chip-qRT-PCR results showed that indeed FoxM1 binds to this predicted region within Dab2's promoter in brain ECs (Fig. 3d. Control lane). Interestingly, the binding of FoxM1 to the *Dab2* promoter region is decreased when the brain ECs were treated with high-concentration glucose or the FoxM1 inhibitor FDI-6. More importantly, disrupting of the FoxM1 binding site with CRISPR in BECs also diminished FoxM1 binding significantly. As a control, lysine 14-acetylated histone H3 binding to β-actin and GAPDH promoters did not change significantly in these cells. Taken together, our data demonstrate that FoxM1 directly binding to the promoter region of Dab2 and regulates its transcription.

Loss of Dab2 promotes faster lysosomal degradation of VEGFR2 in high glucose treated ECs

The loss of Dab2 is known to affect various cellular processes, including growth factor receptor? （there is no subject here, whose endocytosis and degradation?） endocytosis and lysosomal degradation (*need references here*). To determine the effect of Dab2 on VEGFR2 signaling, we utilized EC cells isolated from inducible EC specific Dab2-deficient mice (Dab2-EC^{iko}) and conducted immunofluorescence imaging. We analyzed the colocalization of pVEGFR2 with early endosome markers Early Endosome Antigen 1 (EEA1), the early and recycling endosome marker Rab11, and the late endosome/lysosome marker Lysosome-Associated Membrane Protein 1 (LAMP1) in ECs after VEGFA stimulation. We found that the colocalization of VEGFR2 with EEA1 and Rab11 was decreased in Dab2-deficient ECs compared to wild-type control ECs at all time points (Fig 4a,b), indicating decreased localization of VEGFR2 in early and recycling endosomes in the absence of Dab2. Conversely, the colocalization of pVEGFR2 with LAMP1 was significantly increased in Dab2-deficient ECs compared to control ECs at all time points (Fig 4a,b), suggesting enhanced lysosomal degradation of VEGFR2 in the absence of Dab2. Furthermore, high glucose treatment in skin ECs was found to inhibit the VEGF-induced recycling of VEGFR2 and increase its colocalization with LAMP1 (Fig 4c).Those results suggest that Dab2 promote the recycling of VEGFR2 recycling back to the plasma membrane and inhibits its lysosome-mediated degradation.

Consistent with the observation of diminished localization of VEGFR2 in early endosomes which is important for VEGFR2 signaling (NCB paper), the deficiency of Dab2 resulted in a considerable reduction in the phosphorylation and activation of pVEGFR2, pAkt, and pERK in ECs isolated

from diabetic Dab2-ECiko mice compared to that from diabetic wild type mice, indicating a reduction in VEGF signaling due to the loss of Dab2. No significant changes were observed in the levels of total VEGFR2, Akt, or ERK (Fig 4d). We next determined inhibition of Dab2 with peptide an inhibitor (DPI) can also hamper Dab2 function and impede VEGF signaling. Wild type mouse endothelial cells were pre-treated with DPI or control peptides for 18 hrs followed by VEGF stimulation. Consistent with Dab2 deleted ECs, the DPI peptide significantly reduced the pVEGFR2, pAkt, and pERK relative to the control peptide (Fig 4f).
Together, these results suggest that Dab2 plays a crucial role in regulating the VEGF-VEGFR2 signaling pathway in ECs by enhancing the recycling of VEGFR2 to the plasma membrane and preventing its lysosomal degradation.

Dab2 plays a critical role in VEGFA-induced proliferation angiogenesis *in vitro*

To further investigate the role of Dab2 in angiogeneis, we isolated brain ECs from wild type and Dab2-ECiko mice and treated them with tamoxifen. Dab2 expression was determined by real-time PCR and western blotting to confirm the deletion of Dab2 in ECs from Dab2-EC^{iKO} after tamoxifen treatment (Supplementary Figure, not done yet). We then performed *in vitro* proliferation (EdU labelling), scratch-wound healing, and endothelial cell tube formation in matrigel in normal or high glucose media in the presence VEGFA. The EdU-positive cells were significantly decreased in Dab2-deficient brain ECs compared to wild type controls (Fig 5a). Moreover, high glucose treatment led to number of EdU-postive cells in wild-type brain ECs compared to that cultured in the media with normal glucose concentration (Fig.5). Notably, high glucose treatment of Dab2-deficient brain ECs further dampened these cells' proliferation (Fig.5a). Likewise, the *in vitro* scratch wound healing assay demonstrated that Dab2-deficient brain EC cells exhibited a slower rate of wound closure compared to wild-type controls (Fig 5b). Interesting, high concentration glucose treatment of wild-type ECs led to blunted scratch wound closure similar to ECs from Dab2-EC^{iKO} mice (Fig.5b) Similarly, the in vitro tube formation assay revealed that Dab2-deficient brain EC cells formed fewer and less organized networks in the presence of VEGFA compared to wild-type controls (Fig 5c,d). More importantly, high glucose treatment of wild-type ECs dampens network formation to the extent similar to ECs from Dab2-EC^{iKO} mice cultured in normal glucose condition (Fig. 5c,d). These findings suggest that Dab2 plays a crucial role in regulating the proliferation and migration of brain ECs under both normal and diabetic conditions. Inhibition of Dab2 expression likely underlies the compromised angiogenic function in ECs exposed to hyperglymia in diabetes mellitus.

Blunted wound healing and neovascularization in diabetic Dab2-deficienct mice

To determine if the pro-angiogenic effects of Dab2 promotes wound healing *in vivo*, we examined the effects of Dab2 deficiency on wound healing under physiological and diabetic

conditons. Wounds were created in the dorsal skin of normal or diabetic WT or EC-iDab2KO mice with a disposable biopsy punch under sterile conditions. Each wound was photographed at the indicated times and analyzed. EC-specific Dab2-deficiency delayed wound healing compared to wild-type mice (Fig 6a, b). Whereas diabetic condition dampened wound healing in wild-type mice, diabetic Dab2-EC^{iKO} mice displayed the slowest wound healing rate among all the groups (Fig.6 a, b). Consistently, CD31-specific immunofluorescence staining of wounds isolated on day 7 post wound creation revealed significantly less vascularization of the wound area in high glucose treated EC-iDab2KO mice (Fig 6c). To test the effect of Dab2 on neovascularization *in vivo*, we subcutaneously implanted matrigel plugs containing VEGFA into Dab2-EC^{iKO} and wild type adult diabetic or control mice to directly examine endothelial cell migration and network formation *in vivo*. Consistently, the Dab2-EC^{iKO} groups showed significant reduced vascularization compared to wild-type controls. Furthermore, Matrigel from diabetic wild-type mice exhibited reduced vascularization to a similar extent of that in Dab2-EC^{iKO} mice. Hyperglycemia in diabetic Dab2-EC^{iKO} mice did not further dampen neovascularization in Matrigel compared to that in non-diabetic Dab2-EC^{iKO} mice (Fig 6d). To further investigate the impact of Dab2-deficiency on angiogenesis, we performed neoangiogenesis induced by VEGFA in cornea using a cornea micropocket assay. Immunofluorescent staining of whole mount cornea with CD31-specific antibody further confirmed the impaired vascularization and revealed reduced vessel density in Dab2-EC^{iKO} , diabetic wild-type and diabetic Dab2-EC^{iKO} mice. (Fig 6e). Specifically, we observed a significant decrease in the number of EdU-positive cells in the cornea of diabetic and Dab2 KO mice, indicating a reduction in the proliferative response to VEGF stimulation. Taken together, those observations demonstrate that Dab2 plays an important role in promoting VEGFA-driven angiogenesis and wound healing *in vivo*.

Restoration of Dab2 Rescues Impaired Angiogenesis and Wound Healing in Diabetic Mice:
To investigate the therapeutic potential of Dab2 restoration in diabetic conditions, we conducted a rescue experiment in streptozotocin (STZ)-induced diabetic mice. We administered Dab2-mRNA encapsulated in lipid nanoparticles conjugated with Lrp1 peptide at a dose of 15 µg/mouse intravenously twice a week during the wound healing period. This treatment was aimed at restoring Dab2 expression, and consequently VEGFR2 signaling, to promote angiogenesis and wound healing.
Diabetic mice treated with Dab2-mRNA nanoparticles exhibited significantly accelerated wound healing compared to untreated diabetic mice. The treated group showed faster wound closure rates, with wounds nearly fully healed by day 7, in contrast to the untreated group, where wounds remained significantly larger (Fig. 7a).
Supporting the in vivo findings, we utilized a Dab2-Lenti system to overexpress Dab2 in Dab2 KO and high glucose-treated primary brain endothelial cells from mice. We performed scratch

assays and tube formation assays to mimic wound healing and angiogenesis in vitro. Cells overexpressing Dab2 exhibited higher proliferative property in EdU assay, increased migration in scratch assays and formed more organized and complex tube-like structures in tube formation assays compared to control cells (Fig. 7b-c). These results confirm the critical role of Dab2 in endothelial cell function and its potential to rescue impaired angiogenic responses in diabetic conditions.

References

1. Saeedi, P. *et al.* Global and regional diabetes prevalence estimates for 2019 and projections for 2030 and 2045: Results from the International Diabetes Federation Diabetes Atlas, 9(th) edition. *Diabetes Res Clin Pract* 157, 107843 (2019).
2. Qi, C., Mao, X., Zhang, Z. & Wu, H. Classification and Differential Diagnosis of Diabetic Nephropathy. *J Diabetes Res* 2017, 8637138 (2017).
3. Alicic, R.Z., Rooney, M.T. & Tuttle, K.R. Diabetic Kidney Disease: Challenges, Progress, and Possibilities. *Clin J Am Soc Nephrol* 12, 2032-2045 (2017).
4. Samsu, N. Diabetic Nephropathy: Challenges in Pathogenesis, Diagnosis, and Treatment. *Biomed Res Int* 2021, 1497449 (2021).
5. Cheng, H. & Harris, R.C. Renal endothelial dysfunction in diabetic nephropathy. *Cardiovasc Hematol Disord Drug Targets* 14, 22-33 (2014).
6. Gilbert, R.E. The endothelium in diabetic nephropathy. *Curr Atheroscler Rep* 16, 410 (2014).
7. Leung, W.K., Gao, L., Siu, P.M. & Lai, C.W. Diabetic nephropathy and endothelial dysfunction: Current and future therapies, and emerging of vascular imaging for preclinical renal-kinetic study. *Life Sci* 166, 121-130 (2016).
8. Sol, M. *et al.* Glomerular Endothelial Cells as Instigators of Glomerular Sclerotic Diseases. *Front Pharmacol* 11, 573557 (2020).
9. Bischoff, J. Endothelial-to-Mesenchymal Transition. *Circ Res* 124, 1163-1165 (2019).
10. Wang, E., Wang, H. & Chakrabarti, S. Endothelial-to-mesenchymal transition: An underappreciated mediator of diabetic complications. *Front Endocrinol (Lausanne)* 14, 1050540 (2023).
11. Alvandi, Z. & Bischoff, J. Endothelial-Mesenchymal Transition in Cardiovascular Disease. *Arterioscler Thromb Vasc Biol* 41, 2357-2369 (2021).
12. Hara, T., Ishida, T., Cangara, H.M. & Hirata, K. Endothelial cell-selective adhesion molecule regulates albuminuria in diabetic nephropathy. *Microvasc Res* 77, 348-355 (2009).
13. Piera-Velazquez, S., Li, Z. & Jimenez, S.A. Role of endothelial-mesenchymal transition (EndoMT) in the pathogenesis of fibrotic disorders. *Am J Pathol* 179, 1074-1080 (2011).

14. Di Benedetto, P. *et al.* Endothelial-to-mesenchymal transition in systemic sclerosis. *Clin Exp Immunol* 205, 12-27 (2021).
15. Jimenez, S.A. Role of endothelial to mesenchymal transition in the pathogenesis of the vascular alterations in systemic sclerosis. *ISRN Rheumatol* 2013, 835948 (2013).
16. Yu, C.H. *et al.* High glucose induced endothelial to mesenchymal transition in human umbilical vein endothelial cell. *Exp Mol Pathol* 102, 377-383 (2017).
17. Fujimoto, M. *et al.* Mice lacking Smad3 are protected against streptozotocin-induced diabetic glomerulopathy. *Biochem Biophys Res Commun* 305, 1002-1007 (2003).
18. Li, J., Qu, X. & Bertram, J.F. Endothelial-myofibroblast transition contributes to the early development of diabetic renal interstitial fibrosis in streptozotocin-induced diabetic mice. *Am J Pathol* 175, 1380-1388 (2009).
19. Zeisberg, E.M., Potenta, S.E., Sugimoto, H., Zeisberg, M. & Kalluri, R. Fibroblasts in kidney fibrosis emerge via endothelial-to-mesenchymal transition. *J Am Soc Nephrol* 19, 2282-2287 (2008).
20. Zeisberg, M. & Kalluri, R. Fibroblasts emerge via epithelial-mesenchymal transition in chronic kidney fibrosis. *Front Biosci* 13, 6991-6998 (2008).
21. Peng, H. *et al.* ROCK1 Induces Endothelial-to-Mesenchymal Transition in Glomeruli to Aggravate Albuminuria in Diabetic Nephropathy. *Sci Rep* 6, 20304 (2016).
22. Liu, F., Zhang, S., Xu, R., Gao, S. & Yin, J. Melatonin Attenuates Endothelial-to-Mesenchymal Transition of Glomerular Endothelial Cells via Regulating miR-497/ROCK in Diabetic Nephropathy. *Kidney Blood Press Res* 43, 1425-1436 (2018).
23. Gil, C.L., Hooker, E. & Larrivee, B. Diabetic Kidney Disease, Endothelial Damage, and Podocyte-Endothelial Crosstalk. *Kidney Med* 3, 105-115 (2021).
24. Sison, K. *et al.* Glomerular structure and function require paracrine, not autocrine, VEGF-VEGFR-2 signaling. *J Am Soc Nephrol* 21, 1691-1701 (2010).
25. Eremina, V. *et al.* VEGF inhibition and renal thrombotic microangiopathy. *N Engl J Med* 358, 1129-1136 (2008).
26. Eremina, V. *et al.* Glomerular-specific alterations of VEGF-A expression lead to distinct congenital and acquired renal diseases. *J Clin Invest* 111, 707-716 (2003).
27. Sivaskandarajah, G.A. *et al.* Vegfa protects the glomerular microvasculature in diabetes. *Diabetes* 61, 2958-2966 (2012).
28. Friehs, I. *et al.* Vascular endothelial growth factor delays onset of failure in pressure-overload hypertrophy through matrix metalloproteinase activation and angiogenesis. *Basic Res Cardiol* 101, 204-213 (2006).
29. Illigens, B.M. *et al.* Vascular Endothelial Growth Factor Prevents Endothelial-to-Mesenchymal Transition in Hypertrophy. *Ann Thorac Surg* 104, 932-939 (2017).
30. Tao, W., Moore, R., Smith, E.R. & Xu, X.X. Endocytosis and Physiology: Insights from Disabled-2 Deficient Mice. *Front Cell Dev Biol* 4, 129 (2016).

31. Lanahan, A.A. *et al.* VEGF receptor 2 endocytic trafficking regulates arterial morphogenesis. *Dev Cell* 18, 713-724 (2010).
32. Sawamiphak, S. *et al.* Ephrin-B2 regulates VEGFR2 function in developmental and tumour angiogenesis. *Nature* 465, 487-491 (2010).
33. Wang, Y. *et al.* Ephrin-B2 controls VEGF-induced angiogenesis and lymphangiogenesis. *Nature* 465, 483-486 (2010).
34. Hayashi, M. *et al.* VE-PTP regulates VEGFR2 activity in stalk cells to establish endothelial cell polarity and lumen formation. *Nat Commun* 4, 1672 (2013).
35. Mellberg, S. *et al.* Transcriptional profiling reveals a critical role for tyrosine phosphatase VE-PTP in regulation of VEGFR2 activity and endothelial cell morphogenesis. *FASEB J* 23, 1490-1502 (2009).
36. Nakayama, M. *et al.* Spatial regulation of VEGF receptor endocytosis in angiogenesis. *Nat Cell Biol* 15, 249-260 (2013).
37. Hou, X., Zaks, T., Langer, R. & Dong, Y. Lipid nanoparticles for mRNA delivery. *Nat Rev Mater* 6, 1078-1094 (2021).
38. Zhu, X. *et al.* Long-circulating siRNA nanoparticles for validating Prohibitin1-targeted non-small cell lung cancer treatment. *Proc Natl Acad Sci U S A* 112, 7779-7784 (2015).
39. Liu, Y. *et al.* Theranostic near-infrared fluorescent nanoplatform for imaging and systemic siRNA delivery to metastatic anaplastic thyroid cancer. *Proc Natl Acad Sci U S A* 113, 7750-7755 (2016).
40. Zhu, X. *et al.* Surface De-PEGylation Controls Nanoparticle-Mediated siRNA Delivery In Vitro and In Vivo. *Theranostics* 7, 1990-2002 (2017).
41. Sorensen, I., Adams, R.H. & Gossler, A. DLL1-mediated Notch activation regulates endothelial identity in mouse fetal arteries. *Blood* 113, 5680-5688 (2009).
42. Islam, M.A. *et al.* Restoration of tumour-growth suppression in vivo via systemic nanoparticle-mediated delivery of PTEN mRNA. *Nat Biomed Eng* 2, 850-864 (2018).
43. Xiao, Y. *et al.* Combining p53 mRNA nanotherapy with immune checkpoint blockade reprograms the immune microenvironment for effective cancer therapy. *Nat Commun* 13, 758 (2022).
44. Yan, Z. *et al.* LyP-1-conjugated doxorubicin-loaded liposomes suppress lymphatic metastasis by inhibiting lymph node metastases and destroying tumor lymphatics. *Nanotechnology* 22, 415103 (2011).
45. Cooper, M.E. *et al.* Increased renal expression of vascular endothelial growth factor (VEGF) and its receptor VEGFR-2 in experimental diabetes. *Diabetes* 48, 2229-2239 (1999).
46. Hovind, P., Tarnow, L., Oestergaard, P.B. & Parving, H.H. Elevated vascular endothelial growth factor in type 1 diabetic patients with diabetic nephropathy. *Kidney Int Suppl* 75, S56-61 (2000).

47. Kalathil, D., John, S. & Nair, A.S. FOXM1 and Cancer: Faulty Cellular Signaling Derails Homeostasis. *Front Oncol* 10, 626836 (2020).
48. Mathelier, A. *et al.* JASPAR 2014: an extensively expanded and updated open-access database of transcription factor binding profiles. *Nucleic Acids Res* 42, D142-147 (2014).
49. Ulhaka, K. *et al.* The Anticancer Effects of FDI-6, a FOXM1 Inhibitor, on Triple Negative Breast Cancer. *Int J Mol Sci* 22 (2021).
50. Wang, S.P. *et al.* FDI-6 inhibits the expression and function of FOXM1 to sensitize BRCA-proficient triple-negative breast cancer cells to Olaparib by regulating cell cycle progression and DNA damage repair. *Cell Death Dis* 12, 1138 (2021).
51. Agarwal, V., Bell, G.W., Nam, J.W. & Bartel, D.P. Predicting effective microRNA target sites in mammalian mRNAs. *Elife* 4 (2015).
52. Li, X., Ye, Y., Wang, B. & Zhao, S. miR-140-5p Aggravates Insulin Resistance via Directly Targeting GYS1 and PPP1CC in Insulin-Resistant HepG2 Cells. *Diabetes Metab Syndr Obes* 14, 2515-2524 (2021).
53. Villard, A., Marchand, L., Thivolet, C. & Rome, S. Diagnostic Value of Cell-free Circulating MicroRNAs for Obesity and Type 2 Diabetes: A Meta-analysis. *J Mol Biomark Diagn* 6 (2015).
54. Krutzfeldt, J. *et al.* Silencing of microRNAs in vivo with 'antagomirs'. *Nature* 438, 685-689 (2005).
55. Lampugnani, M.G., Orsenigo, F., Gagliani, M.C., Tacchetti, C. & Dejana, E. Vascular endothelial cadherin controls VEGFR-2 internalization and signaling from intracellular compartments. *J Cell Biol* 174, 593-604 (2006).
56. Bagchi, S., Fredriksson, R. & Wallen-Mackenzie, A. In Situ Proximity Ligation Assay (PLA). *Methods Mol Biol* 1318, 149-159 (2015).
57. Medici, D., Potenta, S. & Kalluri, R. Transforming growth factor-beta2 promotes Snail-mediated endothelial-mesenchymal transition through convergence of Smad-dependent and Smad-independent signalling. *Biochem J* 437, 515-520 (2011).
58. Penheiter, S.G. *et al.* Type II transforming growth factor-beta receptor recycling is dependent upon the clathrin adaptor protein Dab2. *Mol Biol Cell* 21, 4009-4019 (2010).
59. Hannigan, A. *et al.* Epigenetic downregulation of human disabled homolog 2 switches TGF-beta from a tumor suppressor to a tumor promoter. *J Clin Invest* 120, 2842-2857 (2010).
60. Massague, J. TGF-beta signal transduction. *Annu Rev Biochem* 67, 753-791 (1998).
61. Wrana, J.L., Attisano, L., Wieser, R., Ventura, F. & Massague, J. Mechanism of activation of the TGF-beta receptor. *Nature* 370, 341-347 (1994).
62. Di Guglielmo, G.M., Le Roy, C., Goodfellow, A.F. & Wrana, J.L. Distinct endocytic pathways regulate TGF-beta receptor signalling and turnover. *Nat Cell Biol* 5, 410-421 (2003).
63. Tsukazaki, T., Chiang, T.A., Davison, A.F., Attisano, L. & Wrana, J.L. SARA, a FYVE domain protein that recruits Smad2 to the TGFbeta receptor. *Cell* 95, 779-791 (1998).

64. Zhang, X.L., Topley, N., Ito, T. & Phillips, A. Interleukin-6 regulation of transforming growth factor (TGF)-beta receptor compartmentalization and turnover enhances TGF-beta1 signaling. *J Biol Chem* 280, 12239-12245 (2005).
65. Ito, T., Williams, J.D., Fraser, D. & Phillips, A.O. Hyaluronan attenuates transforming growth factor-beta1-mediated signaling in renal proximal tubular epithelial cells. *Am J Pathol* 164, 1979-1988 (2004).
66. Aisagbonhi, O. *et al.* Experimental myocardial infarction triggers canonical Wnt signaling and endothelial-to-mesenchymal transition. *Dis Model Mech* 4, 469-483 (2011).
67. Correia, A.C., Moonen, J.R., Brinker, M.G. & Krenning, G. FGF2 inhibits endothelial-mesenchymal transition through microRNA-20a-mediated repression of canonical TGF-beta signaling. *J Cell Sci* 129, 569-579 (2016).
68. Widyantoro, B. *et al.* Endothelial cell-derived endothelin-1 promotes cardiac fibrosis in diabetic hearts through stimulation of endothelial-to-mesenchymal transition. *Circulation* 121, 2407-2418 (2010).
69. Harris, E.S. & Nelson, W.J. VE-cadherin: at the front, center, and sides of endothelial cell organization and function. *Curr Opin Cell Biol* 22, 651-658 (2010).
70. Vestweber, D. VE-cadherin: the major endothelial adhesion molecule controlling cellular junctions and blood vessel formation. *Arterioscler Thromb Vasc Biol* 28, 223-232 (2008).
71. Vestweber, D., Winderlich, M., Cagna, G. & Nottebaum, A.F. Cell adhesion dynamics at endothelial junctions: VE-cadherin as a major player. *Trends Cell Biol* 19, 8-15 (2009).
72. Dejana, E., Orsenigo, F. & Lampugnani, M.G. The role of adherens junctions and VE-cadherin in the control of vascular permeability. *J Cell Sci* 121, 2115-2122 (2008).
73. Xiao, K. *et al.* Mechanisms of VE-cadherin processing and degradation in microvascular endothelial cells. *J Biol Chem* 278, 19199-19208 (2003).
74. Xiao, K. *et al.* p120-Catenin regulates clathrin-dependent endocytosis of VE-cadherin. *Mol Biol Cell* 16, 5141-5151 (2005).
75. Murakami, M. *et al.* The FGF system has a key role in regulating vascular integrity. *J Clin Invest* 118, 3355-3366 (2008).
76. Monaghan-Benson, E. & Burridge, K. The regulation of vascular endothelial growth factor-induced microvascular permeability requires Rac and reactive oxygen species. *J Biol Chem* 284, 25602-25611 (2009).
77. Gavard, J. & Gutkind, J.S. VEGF controls endothelial-cell permeability by promoting the beta-arrestin-dependent endocytosis of VE-cadherin. *Nat Cell Biol* 8, 1223-1234 (2006).
78. Yang, D.H., Cai, K.Q., Roland, I.H., Smith, E.R. & Xu, X.X. Disabled-2 is an epithelial surface positioning gene. *J Biol Chem* 282, 13114-13122 (2007).
79. Potter, M.D., Barbero, S. & Cheresh, D.A. Tyrosine phosphorylation of VE-cadherin prevents binding of p120- and beta-catenin and maintains the cellular mesenchymal state. *J Biol Chem* 280, 31906-31912 (2005).

80. Turowski, P. *et al.* Phosphorylation of vascular endothelial cadherin controls lymphocyte emigration. *J Cell Sci* 121, 29-37 (2008).
81. Wallez, Y. *et al.* Src kinase phosphorylates vascular endothelial-cadherin in response to vascular endothelial growth factor: identification of tyrosine 685 as the unique target site. *Oncogene* 26, 1067-1077 (2007).
82. Duong, C.N. *et al.* Interference With ESAM (Endothelial Cell-Selective Adhesion Molecule) Plus Vascular Endothelial-Cadherin Causes Immediate Lethality and Lung-Specific Blood Coagulation. *Arterioscler Thromb Vasc Biol* 40, 378-393 (2020).
83. Zhang, H. *et al.* The FoxM1 transcription factor is required to maintain pancreatic beta-cell mass. *Mol Endocrinol* 20, 1853-1866 (2006).
84. Zhang, H. *et al.* Gestational diabetes mellitus resulting from impaired beta-cell compensation in the absence of FoxM1, a novel downstream effector of placental lactogen. *Diabetes* 59, 143-152 (2010).
85. Sawaya, A.P. *et al.* FOXM1 network in association with TREM1 suppression regulates NET formation in diabetic foot ulcers. *EMBO Rep* 23, e54558 (2022).
86. Zhong, L. *et al.* Identification of Maturity-Onset Diabetes of the Young Caused by Mutation in FOXM1 via Whole-Exome Sequencing in Northern China. *Front Endocrinol (Lausanne)* 11, 534362 (2020).
87. Shi, H., Wei, J. & He, C. Where, When, and How: Context-Dependent Functions of RNA Methylation Writers, Readers, and Erasers. *Mol Cell* 74, 640-650 (2019).
88. He, F. *et al.* m(6)A RNA hypermethylation-induced BACE2 boosts intracellular calcium release and accelerates tumorigenesis of ocular melanoma. *Mol Ther* 29, 2121-2133 (2021).
89. Kim, J. & Lee, G. Metabolic Control of m(6)A RNA Modification. *Metabolites* 11 (2021).
90. Feng, C. *et al.* Crystal structures of the human RNA demethylase Alkbh5 reveal basis for substrate recognition. *J Biol Chem* 289, 11571-11583 (2014).
91. Zhang, X. *et al.* Structural insights into FTO's catalytic mechanism for the demethylation of multiple RNA substrates. *Proc Natl Acad Sci U S A* 116, 2919-2924 (2019).
92. Martinez-Reyes, I. *et al.* TCA Cycle and Mitochondrial Membrane Potential Are Necessary for Diverse Biological Functions. *Mol Cell* 61, 199-209 (2016).
93. Zaccara, S., Ries, R.J. & Jaffrey, S.R. Reading, writing and erasing mRNA methylation. *Nat Rev Mol Cell Biol* 20, 608-624 (2019).
94. Chao, Y., Shang, J. & Ji, W. ALKBH5-m(6)A-FOXM1 signaling axis promotes proliferation and invasion of lung adenocarcinoma cells under intermittent hypoxia. *Biochem Biophys Res Commun* 521, 499-506 (2020).
95. Dominissini, D. *et al.* Topology of the human and mouse m6A RNA methylomes revealed by m6A-seq. *Nature* 485, 201-206 (2012).
96. Ratnadiwakara, M. & Anko, M.L. mRNA Stability Assay Using transcription inhibition by Actinomycin D in Mouse Pluripotent Stem Cells. *Bio Protoc* 8, e3072 (2018).

97. Millour, J. *et al.* ATM and p53 regulate FOXM1 expression via E2F in breast cancer epirubicin treatment and resistance. *Mol Cancer Ther* 10, 1046-1058 (2011).
98. Pan, H., Zhu, Y., Wei, W., Shao, S. & Rui, X. Transcription factor FoxM1 is the downstream target of c-Myc and contributes to the development of prostate cancer. *World J Surg Oncol* 16, 59 (2018).
99. Jonas, S. & Izaurralde, E. Towards a molecular understanding of microRNA-mediated gene silencing. *Nat Rev Genet* 16, 421-433 (2015).
100. He, L. & Hannon, G.J. MicroRNAs: small RNAs with a big role in gene regulation. *Nat Rev Genet* 5, 522-531 (2004).
101. Veron, D. *et al.* Podocyte vascular endothelial growth factor (Vegf(1)(6)(4)) overexpression causes severe nodular glomerulosclerosis in a mouse model of type 1 diabetes. *Diabetologia* 54, 1227-1241 (2011).
102. Hohenstein, B. *et al.* Local VEGF activity but not VEGF expression is tightly regulated during diabetic nephropathy in man. *Kidney Int* 69, 1654-1661 (2006).
103. Flyvbjerg, A. *et al.* Amelioration of long-term renal changes in obese type 2 diabetic mice by a neutralizing vascular endothelial growth factor antibody. *Diabetes* 51, 3090-3094 (2002).
104. Sasaki, Y. *et al.* Canonical NF-kappaB activity, dispensable for B cell development, replaces BAFF-receptor signals and promotes B cell proliferation upon activation. *Immunity* 24, 729-739 (2006).
105. Stevens, M. & Oltean, S. Assessment of Kidney Function in Mouse Models of Glomerular Disease. *J Vis Exp* (2018).
106. Danhier, F. *et al.* PLGA-based nanoparticles: an overview of biomedical applications. *J Control Release* 161, 505-522 (2012).
107. Lin, Y.X. *et al.* Reactivation of the tumor suppressor PTEN by mRNA nanoparticles enhances antitumor immunity in preclinical models. *Sci Transl Med* 13 (2021).
108. Luo, G. *et al.* LyP-1-conjugated nanoparticles for targeting drug delivery to lymphatic metastatic tumors. *Int J Pharm* 385, 150-156 (2010).

109. Mathews, C.E., Langley, S.H. & Leiter, E.H. New mouse model to study islet transplantation in insulin-dependent diabetes mellitus. *Transplantation* 73, 1333-1336 (2002).
110. Coleman, D.L. Obese and diabetes: two mutant genes causing diabetes-obesity syndromes in mice. *Diabetologia* 14, 141-148 (1978).
111. Damasceno, D.C. *et al.* Streptozotocin-induced diabetes models: pathophysiological mechanisms and fetal outcomes. *Biomed Res Int* 2014, 819065 (2014).

Figure Legends

Figure 1. High concentration of glucose treatment of ECs down-regulates the expression of Dab2, FoxM1, as well as genes involved in cell cycle progression, cell growth and survival, glycolysis and OXPHOS. The volcano plot illustrates the differentially expressed genes in high glucose (HG) vs control mice brain endothelial cells (Fig 1a) and differentially expressed transcription factors (Fig 1b). The x-axis shows the log2 fold change (log2FC) and the y-axis represents the negative logarithm of the p-value (-log10 p-value). The differentially expressed genes are represented by dots in the plot. Genes with a log2FC greater than 1 and a p-value less than 0.05 are colored in red (up-regulated) or blue (down-regulated). Differential gene expression from RNA-seq was analyzed using GSEA Hallmark geneset (Fig 1c). Geneset enrichment with nominal p-value <0.05 and FDR <0.25 were included. Normalized Enrichment Score (NES) for all gene set with statistical significance, as well as enrichment plot for KEGG cell cycle is shown (Fig 1d).

Figure 2. Expression of FoxM1 and Dab2 is suppressed EC from Diabetic mice and High Glucose treated ECs. qRT-PCR of Dab2 in Brain ECs treated with high and low glucose media for 24 hours (a) and (b) brain and skin ECs isolated from WT and diabetic mice [n = 3, error bars ± SEM (*P < 0.05)]. (c) qRT-PCR of FoxM1 in Brain ECs treated with high and low glucose media for 24 hours [n = 3, error bars ± SEM (*P < 0.05)].
(e) Representative Dab2 western blots in ECs grown in euglycemic and hyperglycemic media [n = 5, error bars ± SEM (*P < 0.05)]. Immunofluorescence staining of Dab2 (green) and CD31 (red) in endothelial cells treated with high and low glucose media for 24 hours (g) and blood vessels grown in matrigel implanted in both wild-type and diabetic mice (h).

Figure 3. FoxM1 directly binds to *Dab2* promoter region and regulates its expression. The immunofluorescence images show the expression of VEGFR2 (green), Dab2 (red) and, FoxM1 (red) in brain endothelial cells from control and FDI-6 treated mice (a). The images were captured at 20x magnification. (b) Effect of FDI-6 on VEGFA-induced VEGFR2 signaling in brain endothelial cells evaluated by Western blot analysis. Brain endothelial cells were treated with FDI-6 for 18 hours followed by VEGFA treatment for 10 minutes. The expression of key VEGFR2 signaling proteins, including VEGFR2, pVEGFR2, Akt, pAkt, ERK, and pERK, was assessed by Western blot analysis. Actin was used as a loading control. (c) The bioinformatic analysis of Dab2 promoter reveals the presence of FoxM1 binding sites with a high peak. The x-axis represents the genomic region of the Dab2 promoter, while the y-axis shows the peak height of the FoxM1 binding sites. (d) ChIP qPCR analysis to examine FOXM1 binding to the Dab2 promoter in response to high glucose, FDI-6 treatment and in cells with a CRISPR mutation in the Foxm1 binding site on the Dab2 promoter. Chromatin was extracted by sonication of cell nuclei and immunoprecipitated with an anti-FOXM1 antibody. Nuclear FoxM1 immunoprecipitates were subjected to qPCR using primers specific for the Dab2 sites. (e) The graphical image shows a the FoxM1 binding motif on the Dab2 promoter.

Figure 4. Loss of Dab2 promotes faster lysosomal degradation of VEGFR2 in high glucose treated ECs. (a) Co-localization of VEGFR2 with EEA1, Rab11 and LAMP1 in Diabetic-WT and

Diabetic-Dab2-KO ECs after VEGF induction. VEGFR2 (green), LAMP1 (red), EEA1 (red) and DAPI (blue) were stained and imaged by immunofluorescence microscopy after 10 min of VEGFA induction and (b) bar graph for colocalization analysis. (c) Western blot analysis of brain endothelial cells (ECs) from diabetic wild-type (WT) and diabetic Dab2-knockout (Dab2KO) mice was performed to evaluate VEGFR2 signaling proteins, including VEGFR2, pVEGFR2, Akt, pAkt, ERK, and pERK. GAPDH was used as a loading control. (d) Representative image of WT and Dab2-KO ECs after 10 min and (e) 15 min of VEGF induction. VEGFR2 (green), LAMP1 (red), EEA1 (red) and DAPI (blue) were stained and imaged by immunofluorescence microscopy. Colocalization of VEGFR2 with lysosomes was observed by merging the VEGFR2 and LAMP1 channels, shown in yellow. Knockout of Dab2 resulted in increased colocalization of VEGFR2 with LAMP1 at both time points, indicating faster lysosomal degradation of VEGFR2 in Dab2-KO ECs. These results support the conclusion that Dab2 is necessary for VEGF-induced VEGFR2 recycling and signaling in ECs. (f) WB analysis of VEGF signaling and growth factor-stimulated phospho-VEGFR2, Akt, and ERK protein levels in WT ECs in presence or absence of inhibitory peptides. Cells were treated with or without inhibitory peptides for 18 hours and stimulated with growth factors. The protein levels of pVEGFR2, Akt, and ERK were analyzed by Western blotting. The results showed that inhibitory peptides significantly reduced the levels of phospho-VEGFR2, Akt, and ERK in WT cells stimulated with growth factors.

Figure 5. Dab2 plays a critical role in VEGFA-induced proliferation angiogenesis *in vitro*. (a) EdU incorporation assay was performed in WT, Dab2 KO, diabetic wild-type and diabetic Dab2 knockout mice brain EC cells in presence of VEGFA. Figure represents images of EdU incorporation (green) and DAPI (blue) staining in brain EC cells of the four groups. (b) Representative images of wound closure in WT-EC monolayers are shown, cultured in the presence of VEGFA and in normal or high glucose-containing media. The scratch assay was performed to evaluate the effect of VEGFA and glucose concentration on the migration and closure of the scratch wound in the endothelial cell monolayers. The images demonstrate the extent of wound closure over time, with differences observed between the experimental conditions. (c) In vitro network formation assay in presence of VEGF for around 10 hours. Mouse brain endothelial cells were plated in matrigel and stimulated with VEGF in the presence or absence of high glucose media. The formation of capillary-like networks was visualized by phase-contrast microscopy. The number of branching points was counted and quantified. The results indicate that inhibition of Dab2 leads to a significant reduction in the number of branching points, suggesting that Dab2 is required for VEGF-induced angiogenic network formation in brain endothelial cells. Data are presented as mean ± SEM, n = 3 independent experiments, *$p < 0.05$ compared to control.

Figure 6. Blunted wound healing and neovascularization in diabetic Dab2-deficienct mice. (a) Wound healing assay in mice with EC-specific Dab2 loss. Circular wounds were created on the back of mice with a disposable biopsy punch under sterile conditions. Each wound was photographed at the indicated times and analyzed. Wound closure analysis (b) showed EC-specific Dab2 loss delayed wound healing compared to WT mice, and diabetes further delayed wound healing in both WT and EC-iDab2 KO mice, respectively, indicating that wounds in diabetic mice with EC-specific Dab2 loss heal the slowest among four groups of mice. (c) CD31-specific immunofluorescence staining of wounds isolated at day 7 revealed significantly less vascularization of the wound area in diabetic EC-iDab2KO mice. (d) Immunofluorescent staining of cryosections from the matrigel plugs with CD31-specific antibody. matrigel plugs containing VEGF was subcutaneously implanted into Dab2-KO and wild type adult diabetic or control mice to directly examine network formation. The Dab2-KO groups showed significantly less angiogenic effects on the matrigel, resulting in reduced vascularization. (d) Retinal micropocket assay to assess the effect of Dab2 deletion on angiogenesis. Retinas of diabetic or normal WT or EC-iDab2KO mice were subjected to the micropocket assay, and pellets containing VEGF were implanted. 20 µM EdU was injected to each mice to stain the proliferating cells. Retinas were collected and stained with CD31 (red) and EdU (green) at day 5 after implantation, with scale bars indicating 100 µm. (e) Quantification of the number of angiogenic sprouts, tip cells originating from the pellet. The number of sprouts and vessel density was reduced in diabetic EC-iDab2KO mice compared to other groups.

Figure 7. Restoration of Dab2 Rescues Impaired Angiogenesis and Wound Healing in Diabetic Mice (a) Visual comparison of wound healing in diabetic mice induced with streptozotocin (STZ) and subsequently treated with Dab2-loaded LNPs versus those without LNP treatment. The images show the progression of wound closure over time, with distinct panels depicting wound states at specific time intervals post-injury. The left panel illustrates the healing process in STZ-treated mice without Dab2-LNP intervention, while the right panel shows the accelerated wound healing observed in mice receiving Dab2-LNP treatment. Measurements of wound size reduction are quantitatively presented below each image set to highlight the enhanced healing rate in the Dab2-LNP treated group. (b) Figure displays the results of a scratch migration assay in primary ECs, comparing the effects of high glucose treatment alone to high glucose treatment combined with Dab2-Lenti. The top panel shows ECs exposed to high glucose, illustrating their baseline migratory response in the scratch assay. The bottom panel reveals a noticeably enhanced migration in ECs treated with both high glucose and Dab2-Lenti, as indicated by the more significant closure of the scratch area. The figure quantitatively contrasts the migration distances between the two conditions, emphasizing the role of Dab2-Lenti in improving EC migration under hyperglycemic conditions. (c) figure illustrates the results of an EdU proliferation assay comparing primary ECs treated with high glucose conditions to those

treated with both high glucose and Dab2-Lenti. The series of images capture EdU incorporation, indicative of cell proliferation, in both experimental groups. The top panel showcases ECs under high glucose treatment alone, displaying a baseline level of proliferation. The bottom panel demonstrates enhanced cellular proliferation in ECs treated with high glucose and Dab2-Lenti, as evidenced by the increased incorporation of EdU. Quantitative data below the images provide a clear comparison of the proliferation rates between the two groups, highlighting the effect of Dab2-Lenti treatment in promoting cell growth under hyperglycemic conditions.

This graphical abstract depicts the effect of diabetes on endothelial cells (ECs) and angiogenesis. In normal ECs, FoxM1 binds to the Dab2 promoter in the nucleus, promoting Dab2 transcription. Dab2, in turn, promotes angiogenesis by recycling activated VEGFR2 to the plasma membrane. However, in diabetic ECs, FoxM1 is low, leading to down-regulation of Dab2 transcription. As a result, VEGFR2 recycling is impaired upon VEGFA induction, reducing angiogenesis in diabetes and leading to impaired wound healing.

1

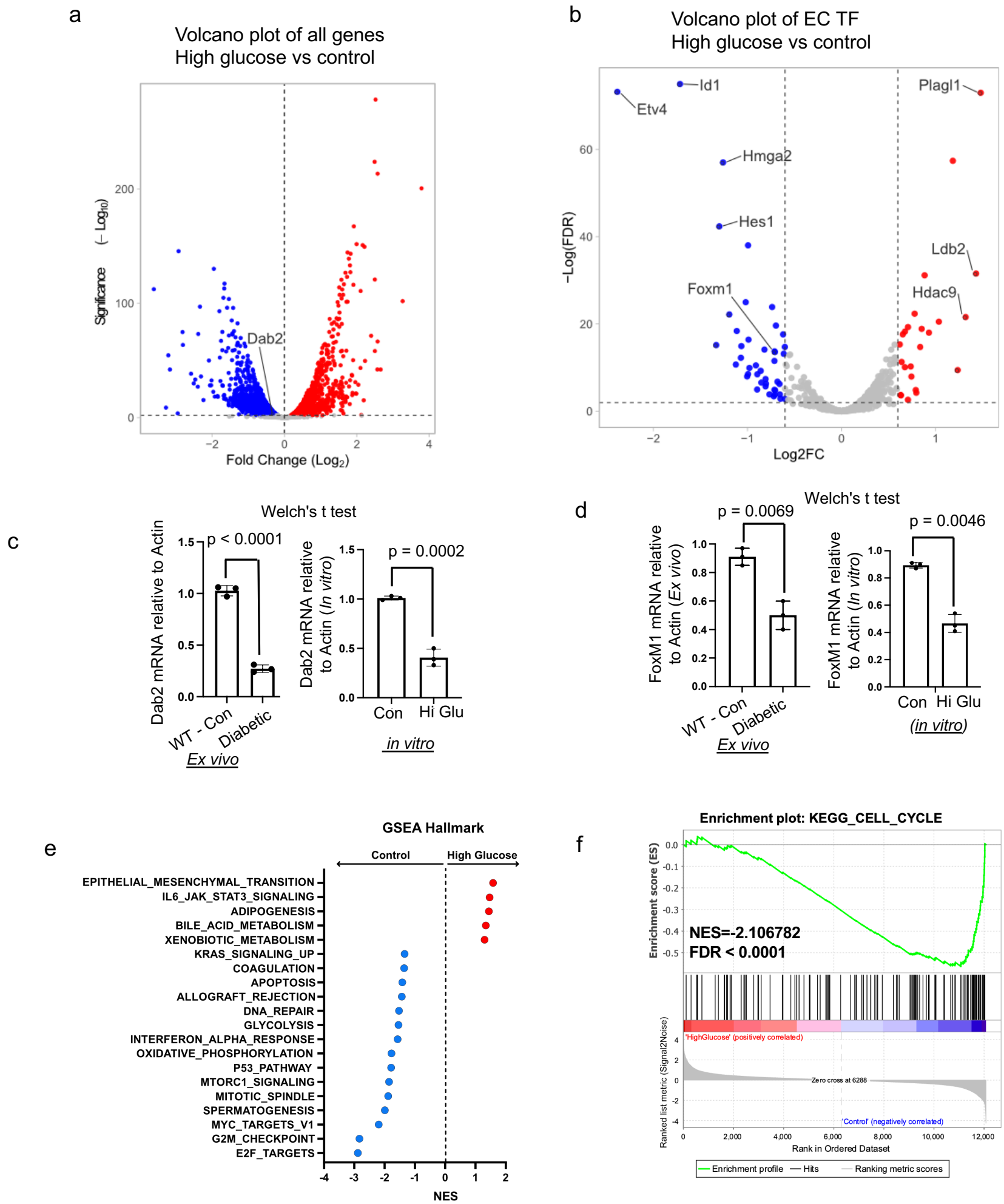

High concentration of glucose treatment of ECs down-regulates the expression of Dab2, FoxM1, as well as genes involved in cell cycle progression, cell growth and survival, glycolysis and OXPHOS

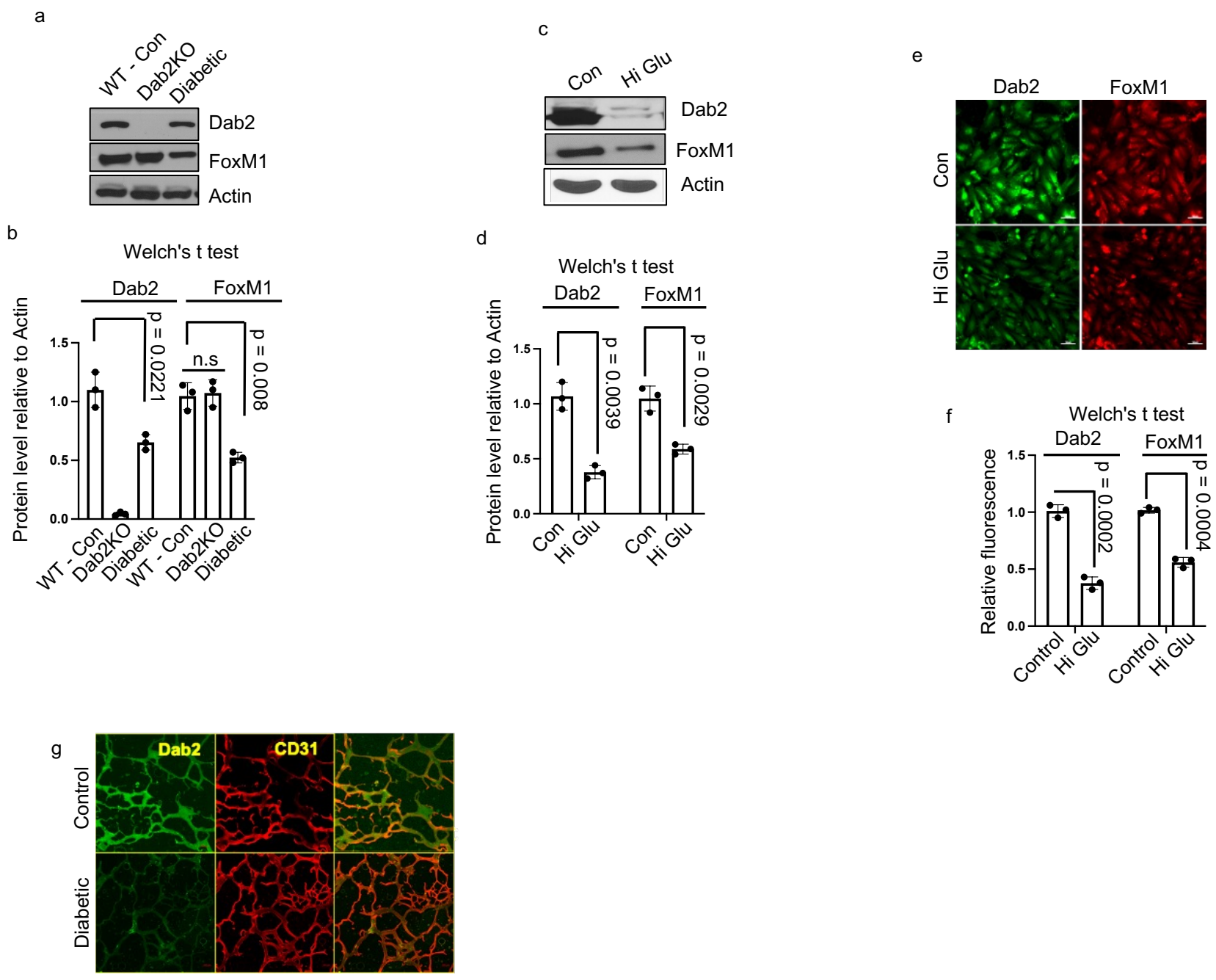

Expression of FoxM1 and Dab2 is suppressed EC from Diabetic mice and High Glucose treated ECs

3

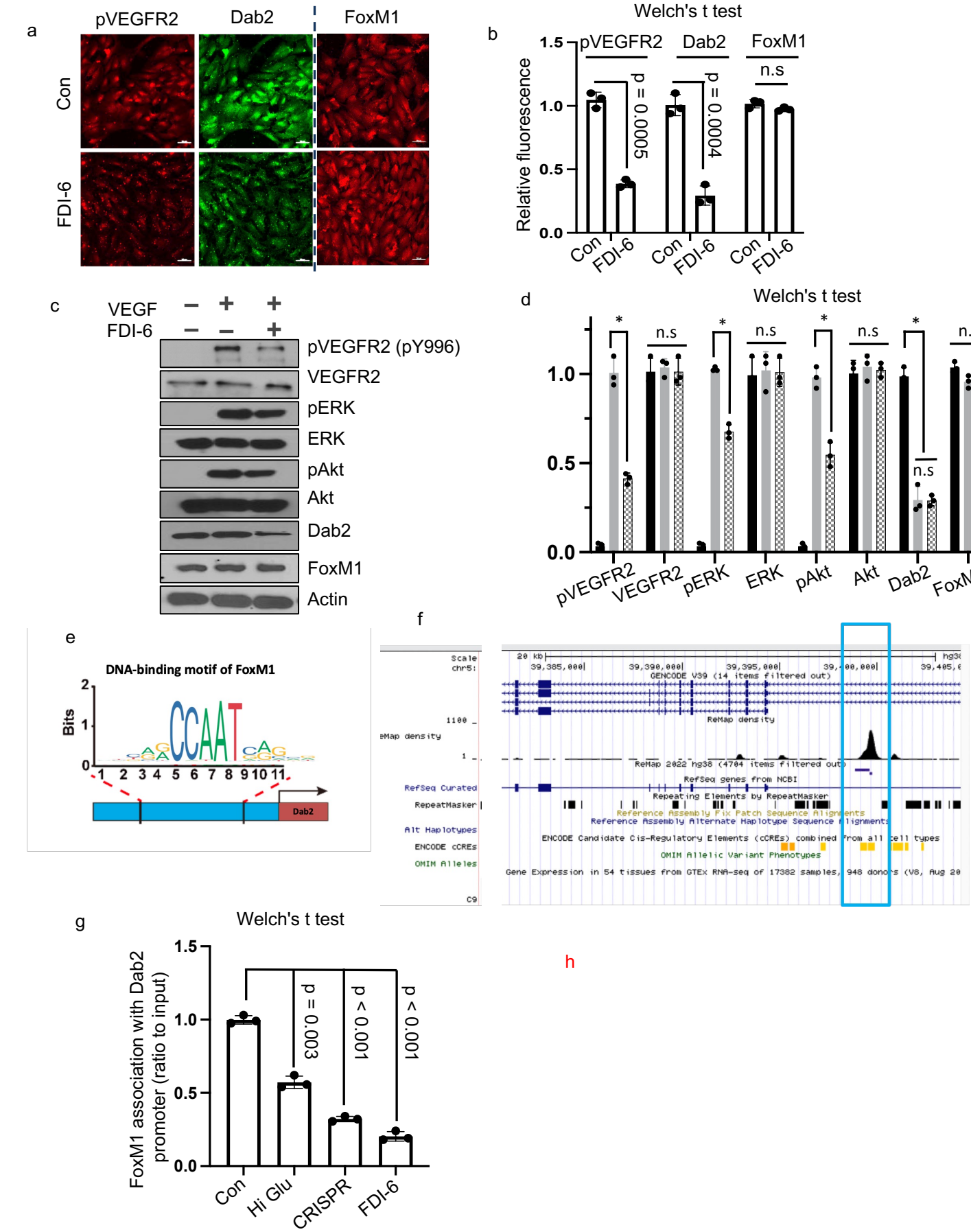

FoxM1 directly binds to *Dab2* promoter region and regulates its expression

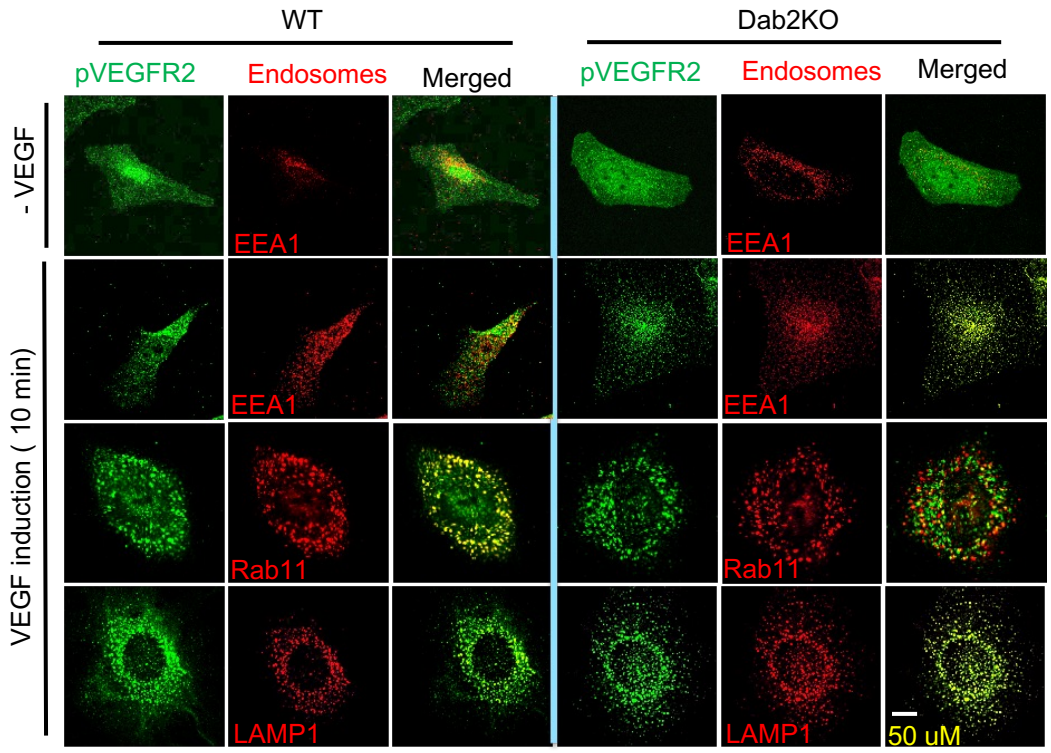
a
WT
Dab2KO
pVEGFR2
Endosomes
Merged
pVEGFR2
Endosomes
Merged
- VEGF
VEGF induction (10 min)
EEA1
EEA1
EEA1
EEA1
Rab11
Rab11
LAMP1
LAMP1
50 uM

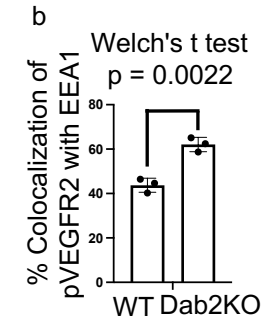
b
Welch's t test
p = 0.0022
% Colocalization of pVEGFR2 with EEA1
80
60
40
20
0
WT
Dab2KO

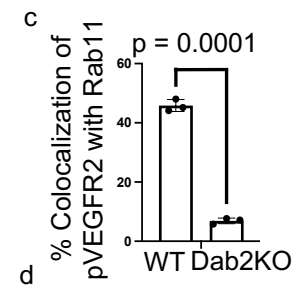
c
p = 0.0001
% Colocalization of pVEGFR2 with Rab11
60
40
20
0
WT
Dab2KO

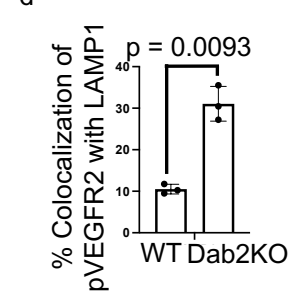
d
p = 0.0093
% Colocalization of pVEGFR2 with LAMP1
40
30
20
10
0
WT
Dab2KO

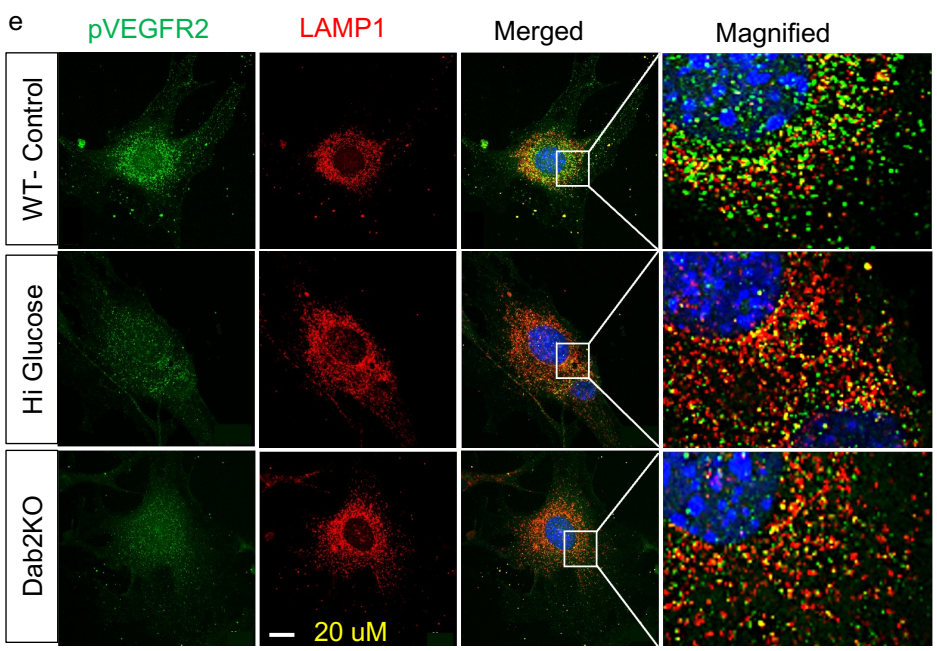
e
pVEGFR2
LAMP1
Merged
Magnified
WT- Control
Hi Glucose
Dab2KO
20 uM

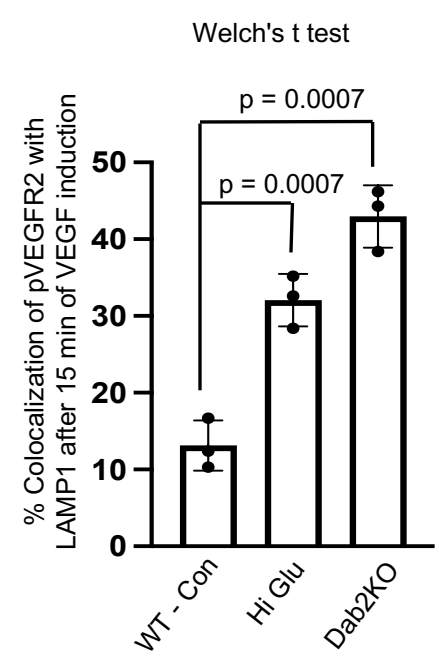
f
Welch's t test
p = 0.0007
p = 0.0007
% Colocalization of pVEGFR2 with LAMP1 after 15 min of VEGF induction
50
40
30
20
10
0
WT - Con
Hi Glu
Dab2KO

5

a

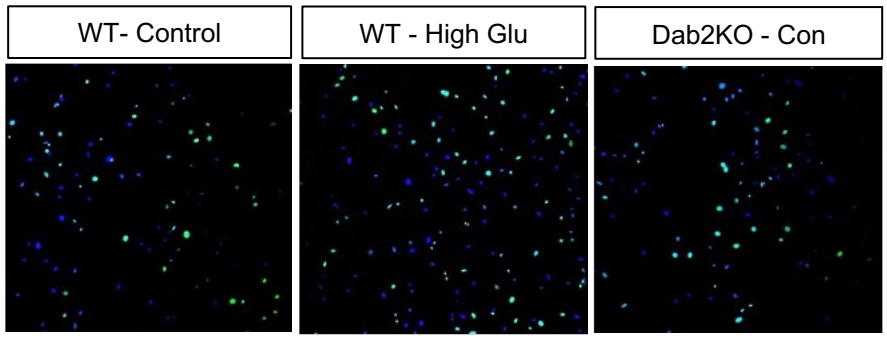

b

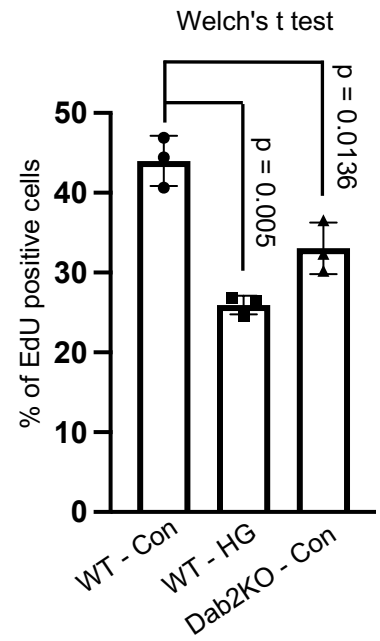

c

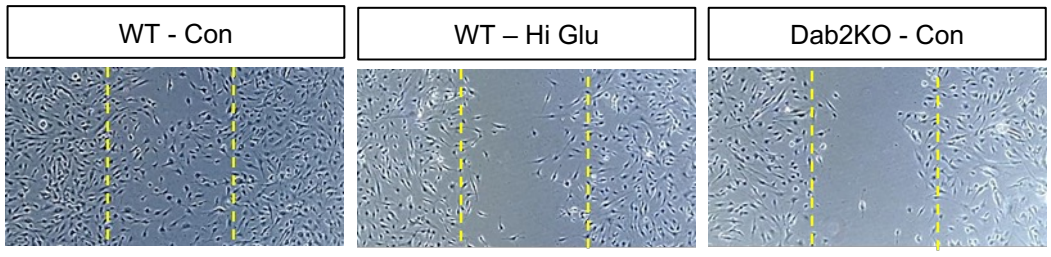

d

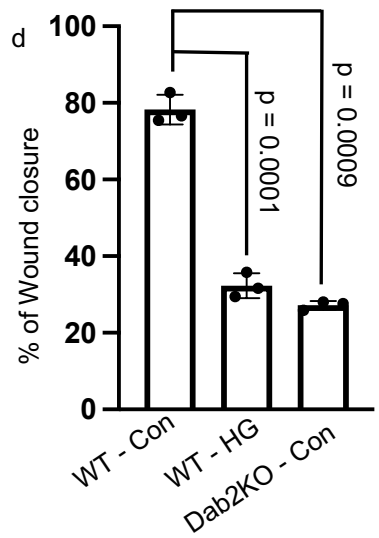

e

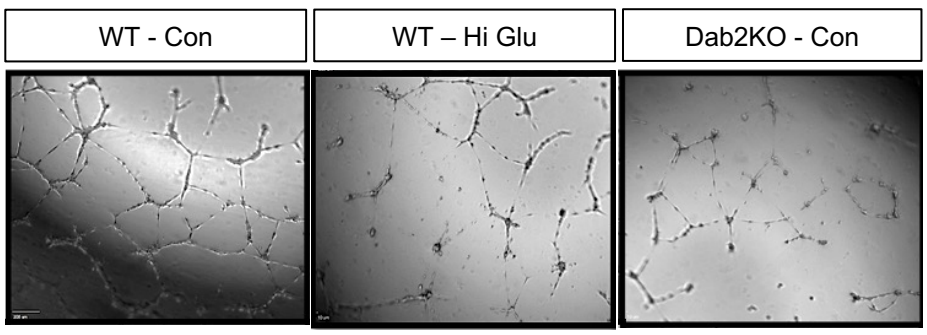

f

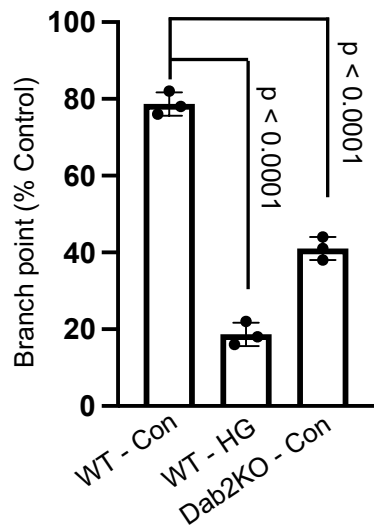

Dab2 plays a critical role in VEGFA-induced proliferation angiogenesis *in vitro*

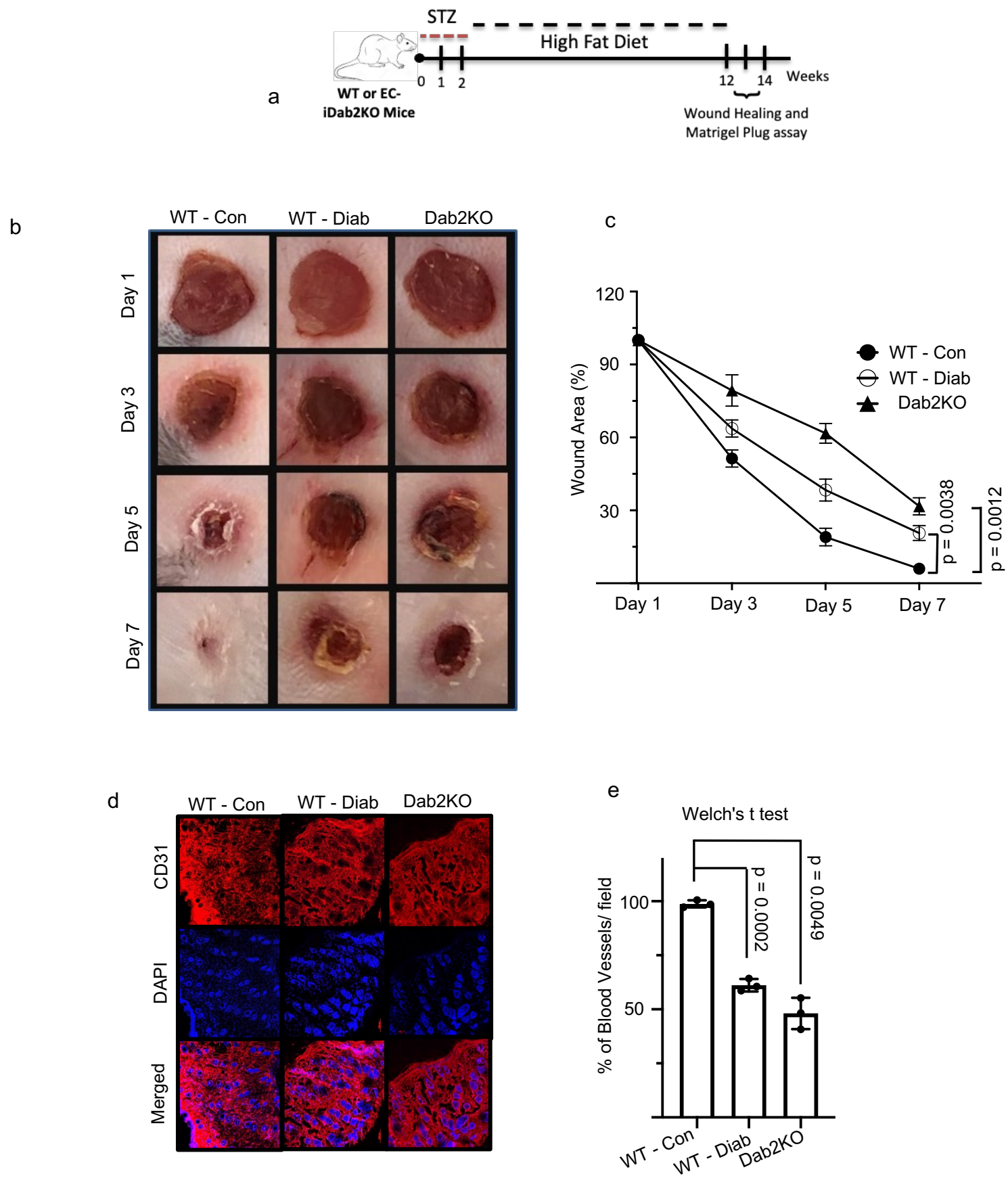

Blunted wound healing and neovascularization in diabetic Dab2-deficient mice

f

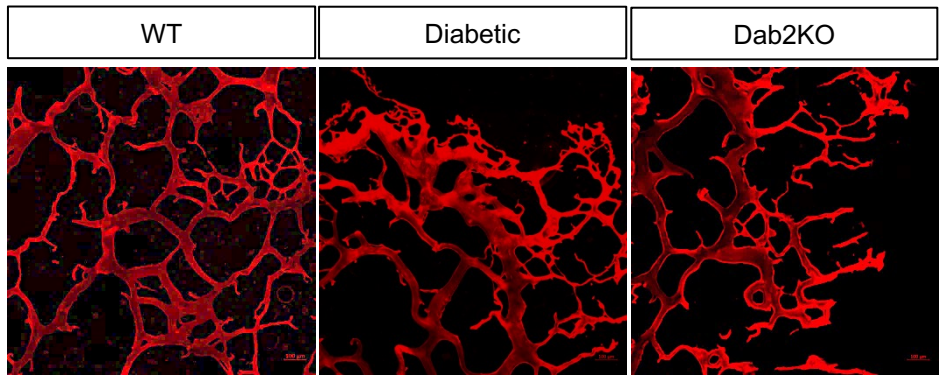
WT
Diabetic
Dab2KO

g

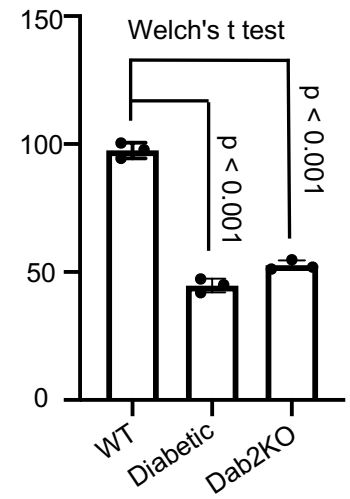
Welch's t test
150
100
50
0
p < 0.001
p < 0.001
WT
Diabetic
Dab2KO

h

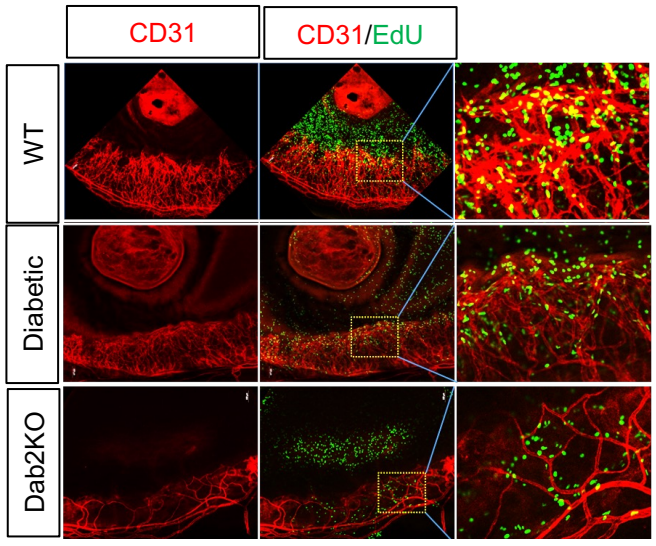
CD31
CD31/EdU
WT
Diabetic
Dab2KO

i

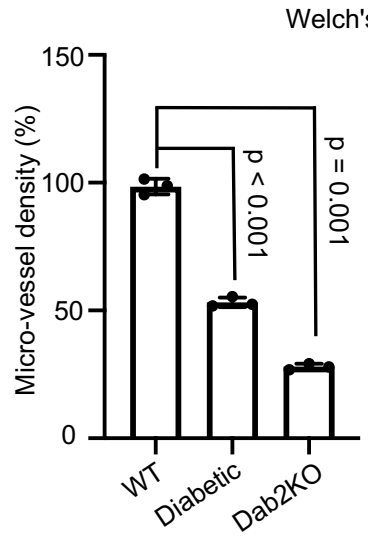
Welch's t test
Micro-vessel density (%)
150
100
50
0
p < 0.001
p = 0.001
WT
Diabetic
Dab2KO

j

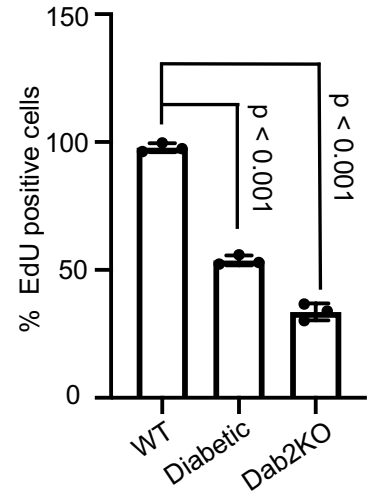
% EdU positive cells
150
100
50
0
p < 0.001
p < 0.001
WT
Diabetic
Dab2KO

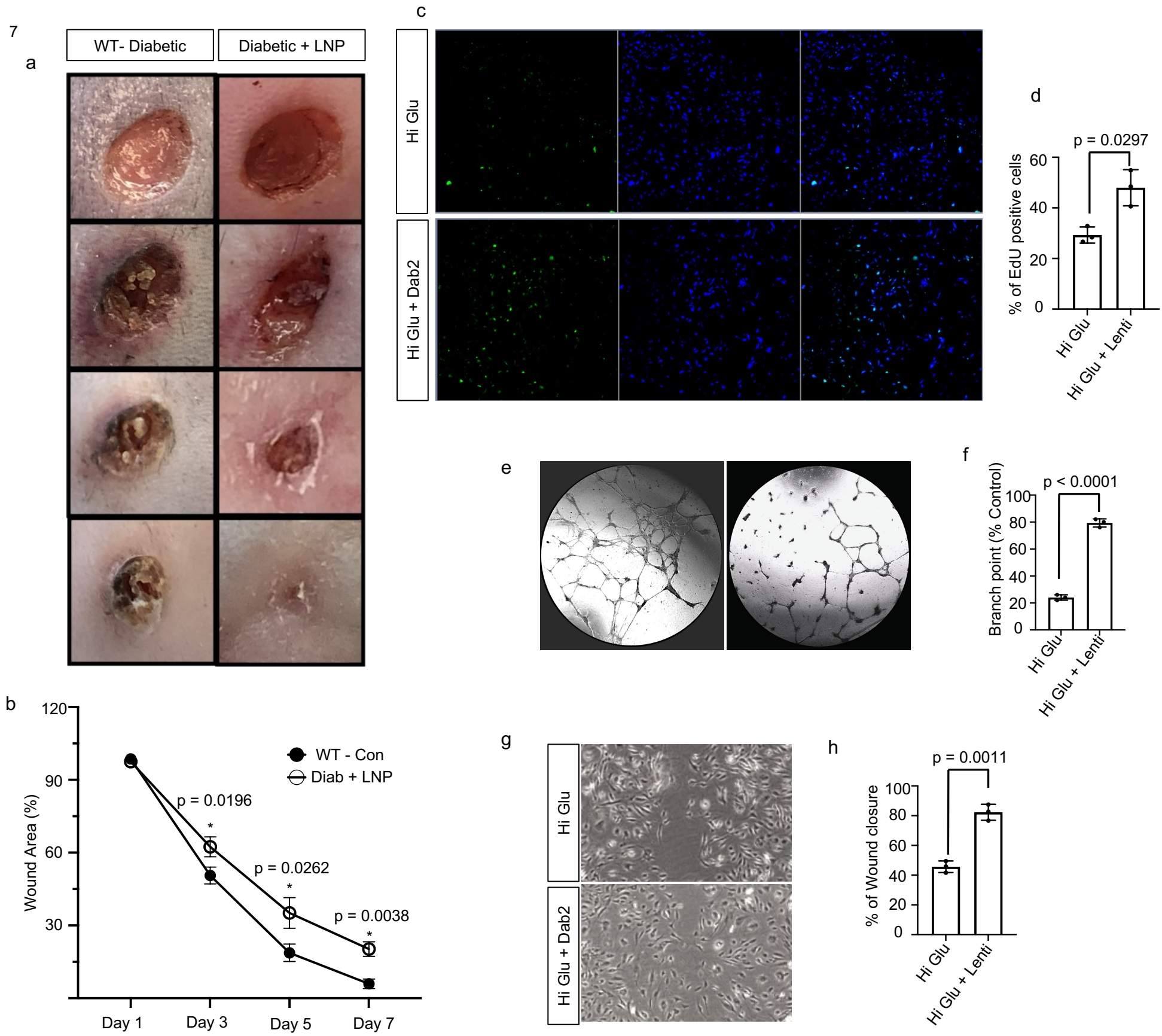

Restoration of Dab2 Rescues Impaired Angiogenesis and Wound Healing in Diabetic Mice
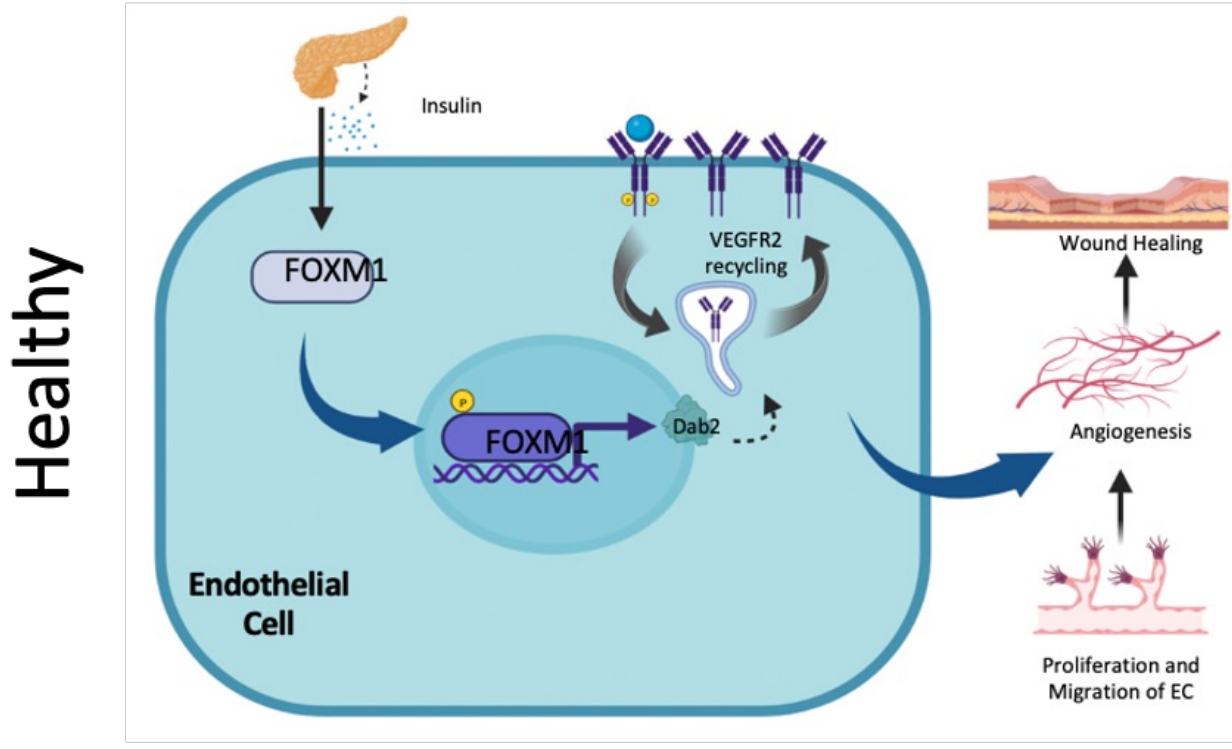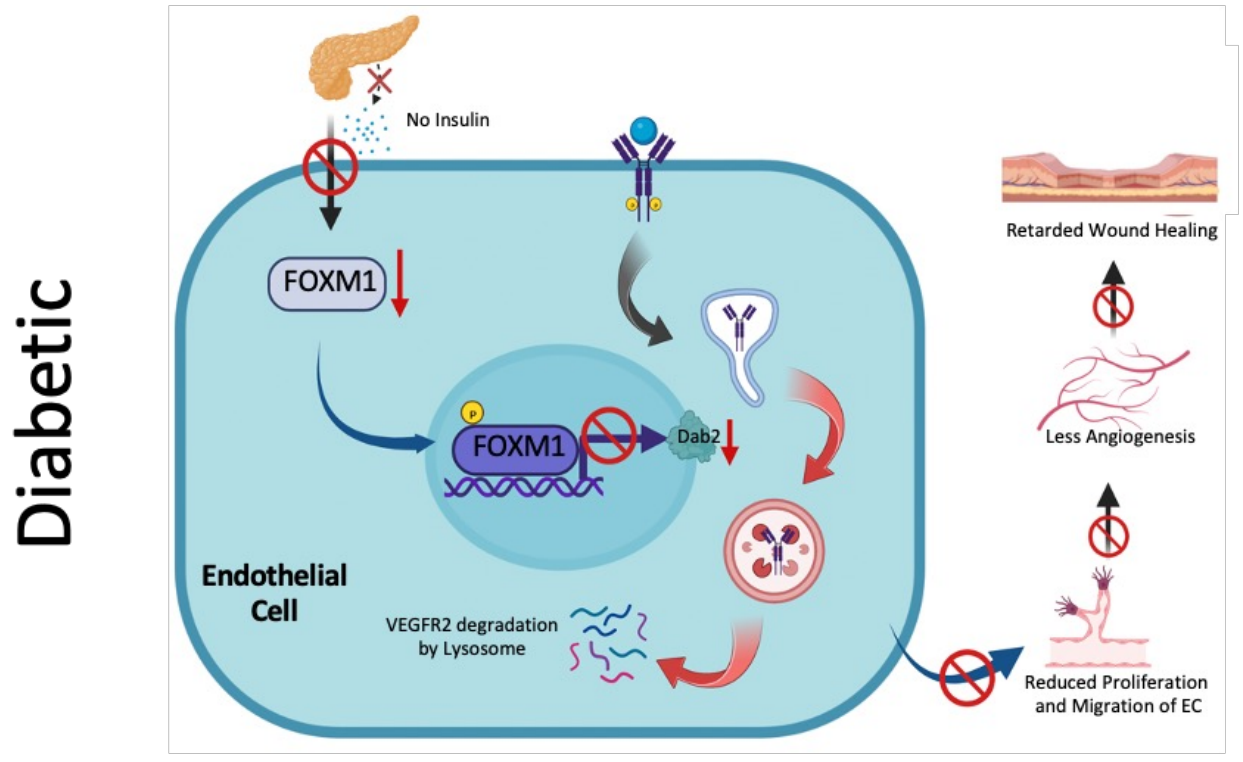
Graphical Abstract